Miner Deposita (2015) 50:159–186
DOI 10.1007/s00126-014-0528-1

ARTICLE

Enrichment of U–Se–Mo–Re–V in coals preserved within marine carbonate successions: geochemical and mineralogical data from the Late Permian Guiding Coalfield, Guizhou, China

Shifeng Dai · Vladimir V. Seredin · Colin R. Ward · James C. Hower · Yunwei Xing · Weiguo Zhang · Weijiao Song · Peipei Wang

Received: 11 February 2014 / Accepted: 11 May 2014 / Published online: 13 June 2014

Abstract We present multi-element data on the super-high-organic-sulfur (SHOS; 5.19 % on average) coals of Late Permian age from Guiding, in Guizhou Province, China. The coals, formed on restricted carbonate platforms, are all highly enriched in S, U, Se, Mo, Re, V, and Cr, and, to a lesser extent, Ni and Cd. Although the Guiding coals were subjected to seawater influence, boron is very low and mainly occurs in tourmaline and mixed-layer illite/smectite. Uranium, Mo, and V in the coal are mainly associated with the organic matter. In addition, a small proportion of the U occurs in coffinite and brannerite. The major carrier of Se is pyrite rather than marcasite. Rhenium probably occurs in secondary sulfate and carbonate minerals. The U-bearing coal deposits have the following characteristics: the formation age is limited to Late Permian; concentrations of sulfur and rare metals (U, Se, Mo, Re, V, and in some cases, rare earth elements and Y) are highly elevated; the U-bearing coal beds are intercalated with marine carbonate rocks; organic sulfur and rare metals are uniformly distributed within the coal seams; and the combustion products (e.g., fly and bottom ash) derived from the coal deposits may have potential economic significance for rare metals: U, Se, Mo, Re, V, rare earth elements, and Y.

Keywords Super-high-organic-sulfur coal · U–Se–Mo–Re–V enrichment model · Late Permian coals · Marine carbonate succession · Hydrothermal fluids

Editorial handling: B. Lehmann

Electronic supplementary material The online version of this article (doi:10.1007/s00126-014-0528-1) contains supplementary material, which is available to authorized users.

S. Dai (✉) · Y. Xing · W. Zhang · W. Song · P. Wang
State Key Laboratory of Coal Resources and Safe Mining, China University of Mining and Technology (Beijing), Beijing 100083, China
e-mail: daishifeng@gmail.com

V. V. Seredin
Institute of Geology of Ore Deposits, Petrography, Mineralogy, and Geochemistry, Russian Academy of Sciences, Staromonetnyi per. 35, Moscow 119017, Russia

C. R. Ward
School of Biological, Earth and Environmental Sciences, University of New South Wales, Sydney NSW 2052, Australia

J. C. Hower
Center for Applied Energy Research, University of Kentucky, 2540 Research Park Drive, Lexington, KY 40511, USA

Introduction

Coals preserved within marine carbonate successions have been found in the Guiding (Guizhou Province), Yanshan (Yunnan Province), Heshan (Guangxi Province), and Chenxi (Hunan Province) coalfields in southern China (Fig. 1a). The coals are intercalated with marine carbonate rocks (Hou et al. 1995; Lei et al. 1994; Shao et al. 2003; Zeng et al. 2005) and most of them are classified as super-high-organic-sulfur (SHOS) coals; these are a special class of coal that is remarkably enriched in organic sulfur, usually in the range of 4 to 11 % (Chou 1997a, 2012). Such SHOS coals are not very common, but have both practical and academic research significance. From a practical perspective, SHOS coals usually contain highly elevated concentrations of several elements, including U, Se, Mo, V, Re, and, in some cases, rare earth elements and Y (REY, or REE if Y is not included), which could potentially be utilized from the coal combustion by-products, e.g., fly ash (Dai et al. 2013a; Seredin and Finkelman 2008). From an academic perspective, the mechanism of SHOS coal formation and the enrichment of trace elements and minerals in such coals could enhance the

understanding of the paleoenvironmental evolution and regional tectonic evolution (Greb 2013).

Previous studies have investigated the depositional environment of the Heshan Coalfield (Chen 1987; Huang et al. 1994; Jin and Li 1987); the geochemistry of organic sulfur in the Guiding Coalfield (Chou 1997a, 2004; Hou et al. 1995; Lei et al. 1994); and the mineralogy and trace-element geochemistry in the Yanshan, Heshan, Fusui, and Chenxi coalfields (Dai et al. 2008, 2013a; Li and Tang 2013; Li et al. 2013; Shao et al. 2003; Zeng et al. 2005), and made preliminary estimations of the potential for utilization of rare earth elements and yttrium in SHOS coals of the Heshan and Fusui coalfields (Dai et al. 2013a, b). These studies have variously attributed the highly elevated sulfur and U–Se–Mo–Re–V concentrations to a marine transgressive environment (Shao et al. 2003; Li and Tang 2013; Li et al. 2013), hydrothermal fluids (including those of submarine exhalation; Dai et al. 2008, 2013a,b), and the formation of soil horizons prior to peat accumulation (Zeng et al. 2005).

Although studies have been carried out on the geochemistry of the organic sulfur in the coal (Lei et al. 1994), the trace element abundances and mineral compositions of the Guiding SHOS coals have not previously been investigated. In this paper, we report an investigation of the geological factors that may have influenced the geochemical and mineralogical anomalies observed in the Guiding coals. In addition to combining previously reported trace element data on SHOS coals from the Yanshan, Heshan, and Chenxi coalfields, the general occurrence of this U-bearing deposit body and the geochemical characteristics of the U–Se–Mo–Re–V enrichment assemblage are discussed.

Geological setting

The Guiding Coalfield is located in the middle of Guizhou Province, southwestern China (Fig. 1a). The sedimentary sequences in the coalfield (Fig. 2) include the Lower Permian Maokou Formation, Upper Permian Wujiaping Formation, Lower Triassic Daye Formation, and Quaternary deposits.

The Maokou Formation is made up of thick, gray limestone layers containing algal fossil debris. The coal-bearing unit in the Guiding Coalfield is the Wujiaping Formation, overlying the limestones of the Maokou Formation with an unconformable contact. The Wujiaping Formation is mainly composed of flint-bearing limestones interlayered with coal and thin layers of mudstone and siliceous rock layers. Three different parts can be identified in the vertical section of the Wujiaping Formation. The lower part, with an average thickness of 60 m, is composed of medium-thick flint-bearing limestone interlayered with silty mudstone. The middle part has an average thickness of 80 m and is dominated by interbedded thin siliceous rocks and thin silty mudstones. The M3 seam, the major workable seam, with an average thickness of 0.9 m, is located in the upper

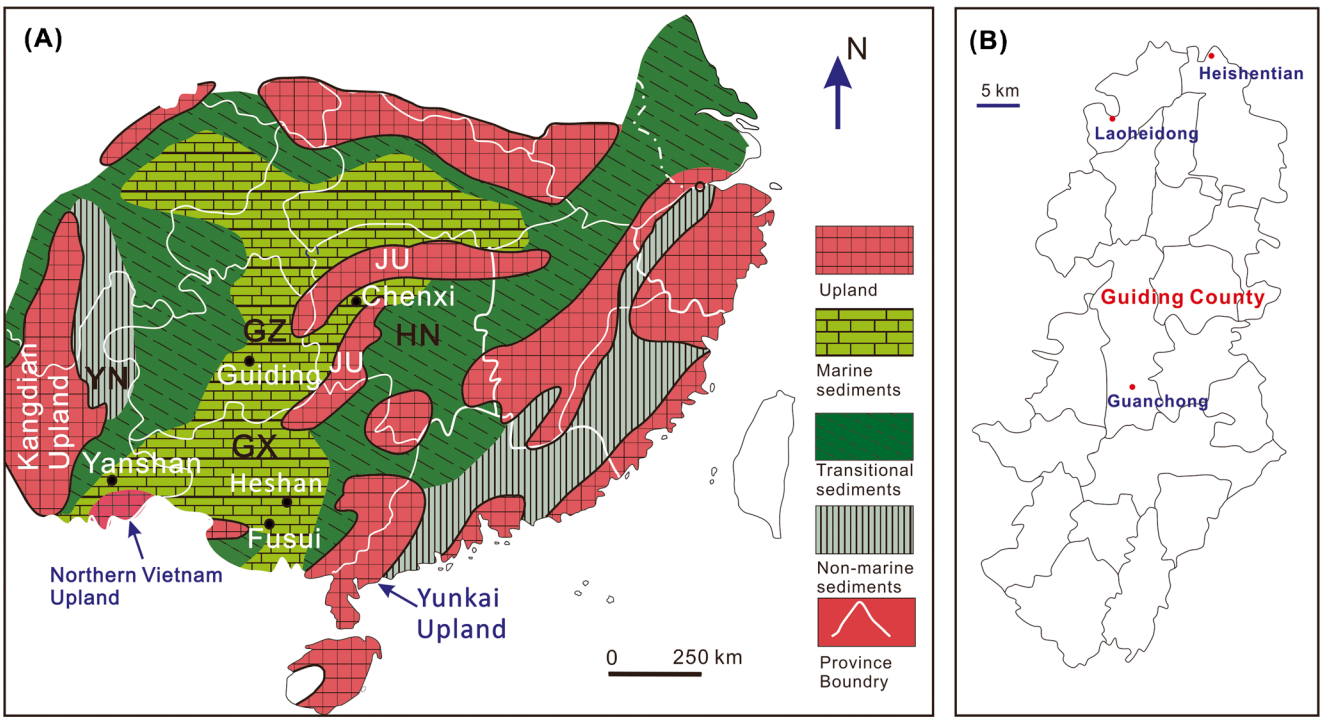

Fig. 1 Paleoenvironment and location of the Guiding, Yanshan, Heshan, Fusui, and Chenxi coalfields in southwestern China (**a**) and the sampling locations in Guiding county (**b**). *JU*, Jiangnan Upland. *GZ*, Guizhou Province; *GX*, Guangxi Province; *YN*, Yunnan Province; *HN*, Hunan Province

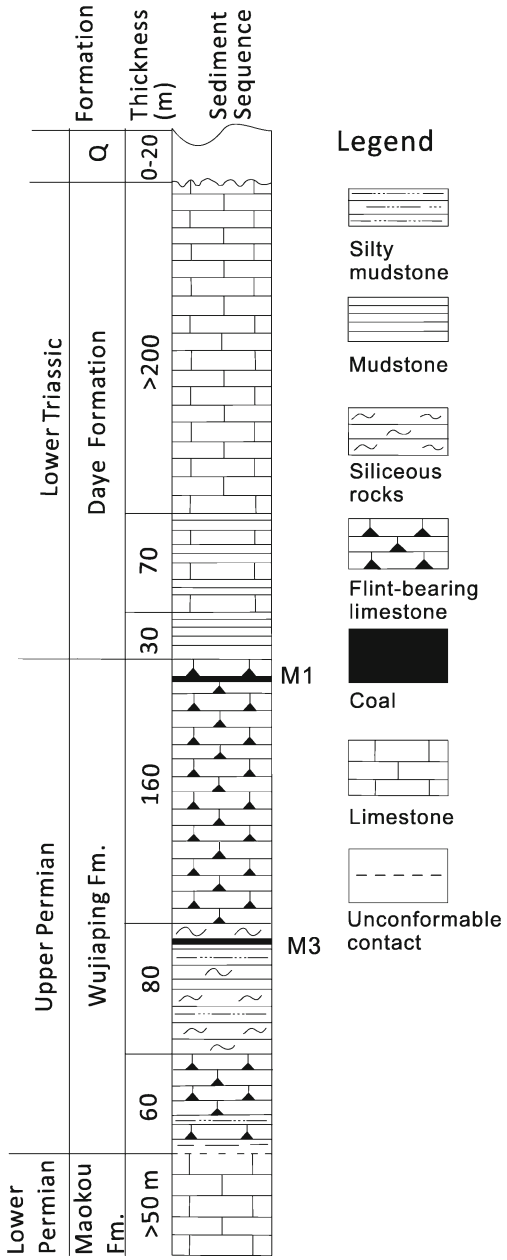

Fig. 2 Sedimentary sequences in the Guiding Coalfield. *Q*, Quarternary; *Fm.*, Formation

portion of this middle part. The upper part of the Wujiaping Formation, with an average thickness of 160 m, largely consists of flint-bearing limestone. The M1 seam, with an average thickness of 20 cm, is located in the uppermost portion of this interval.

The roof and floor strata of the M1 and M3 seams are variable in nature. The roof and floor of the M1 seam both consist of silicified or flint-bearing limestone, although, in some cases, the floor stratum is composed of siliceous rock (chert). The roof stratum of the M3 seam consists of silicified limestone or siliceous rock, and the floor is dominated by siliceous rock.

The overlying Daye Formation can also be divided into three parts based on lithologic composition. The lower part, with an average thickness of 30 m, consists of grayish yellow or brownish yellow mudstone. The middle part has an average thickness of 70 m and is made up of alternating thin limestone and mudstone layers. The upper part has an average thickness greater than 200 m and consists of gray limestone.

The sediment-source region for the Guiding Coalfield was the Kangdian Upland (China National Administration of Coal Geology 1996), which supplied terrigenous materials to most of the Late Permian coal-bearing areas in southwestern China.

Like the Guiding coals, the coals of the Yanshan Coalfield in Yunnan Province (Dai et al. 2008), the Heshan Coalfield in Guangxi Province (Lei et al. 1994; Shao et al. 2003; Zeng et al. 2005), and the Chenxi Coalfield in Hunan Province were formed in tidal flat environments on a restricted carbonate platform (Fig. 1a), and thus were preserved within marine carbonate successions. However, the coal-bearing strata of the Fusui Coalfield, which is located close to the Heshan Coalfield (Fig. 1a), were formed in a lagoonal environment on an open carbonate platform with relatively low-energy hydrodynamics (Dai et al. 2013b; Feng et al. 1994). Although all these coal-bearing strata have different stratigraphic names (e.g., Heshan Formation for the Fusui and Heshan coalfields; Wujiaping Formation for the Yanshan, Guiding, and Chenxi coalfields), they are all of Late Permian age. The roof strata of all the coals have a limestone-dominated composition (limestone, silicified limestone, flint-containing limestone, or bioclastic limestone). In some cases, thin layers of siliceous rock (chert) or mudstone are interlayered between the coal and the limestone-dominated roof strata. The lithologic composition of the floor strata, however, is variable, mostly consisting of limestone, but in some cases of siliceous rock (chert), marl, or mudstone.

Samples and analytical procedures

Samples of coal and non-coal roof and floor strata were collected from three mines in the Guiding Coalfield of Guizhou Province: the Guanchong (GC), Laoheidong (LHD), and Heishentian (HST) mines (Fig. 1b).

Two channel samples from each of the M1 (GC-1C, LHD-1C) and M3 seams (GC-3C, HST-3C), five coal bench samples of the M3 seam from the Guanchong Mine (GC-3-1 to GC-3-5), and three coal bench samples of the M3 seam from the Heishentian Mine (HST-3-0 to HST-3-4), respectively, were taken from the mined fresh coal faces (Table 1). The sample of the M1 seam from the Laoheidong Mine (LHD-1C) was collected from the coal outcrop. Each channel and coal bench sample was cut over an area 10-cm wide and 10-cm deep. The non-coal roof and floor strata samples have suffixes R and F, respectively (see Electronic Supplementary File).

Table 1 Coal seam/bench thickness (cm), proximate and ultimate analyses (%), sulfur (%), calorific values (MJ/kg), and vitrinite random reflectance (%) of the Guiding coals

Sample		Thickness (cm)	M_{ad}	V_{daf}	A_d	C_{daf}	H_{daf}	N_{daf}	$Q_{gr,ad}$	$S_{t,d}$	$S_{p,d}$	$S_{s,d}$	$S_{o,d}$	R_r
Channel	GC-1C	20	1.29	21.7	23.3	84.9	5.06	0.79	26.2	6.55	0.82	0.37	5.37	1.34
	LHD-1C	20	1.56	26.1	16.9	83.9	5.73	0.63	29.2	6.61	0.23	0.69	5.69	1.10
	GC-3C	101	1.33	22.7	23.8	84.9	5.76	0.78	25.8	6.70	0.55	0.5	5.65	1.37
	HST-3C	65	1.90	30.0	23.5	80.2	6.17	0.73	25.8	6.27	1.36	0.39	4.52	0.86
Bench	GC-3-1	5	0.94	36.4	48.2	89.9	5.08	0.96	18.6	4.73	1.15	0.12	3.47	nd
	GC-3-2	20	1.31	22.7	21.0	84.5	5.24	0.79	27.9	6.54	0.36	0.38	5.79	nd
	GC-3-3	20	1.51	20.6	15.1	81.4	4.35	0.72	29.4	6.53	0.07	0.62	5.84	nd
	GC-3-4	20	1.52	20.3	16.3	86.9	6.10	0.76	29.3	7.05	0.10	0.56	6.39	nd
	GC-3-5	36	1.64	18.9	13.9	80.6	3.95	0.69	29.4	7.46	0.14	0.70	6.62	nd
	GC-3B-Av	101	1.49	21.1	17.7	83.2	4.77	0.74	28.6	6.88	0.21	0.56	6.10	nd
	HST-3-0	20	1.90	27.2	43.3	nd	nd	nd	nd	5.84	3.15	0.27	2.42	nd
	HST-3-1	10	1.25	29.1	24.2	79.1	6.28	0.72	25.8	6.11	1.71	0.12	4.27	0.81
	HST-3-2	38	1.17	28.9	14.2	81.5	5.13	0.73	30.0	6.36	0.72	0.23	5.42	0.92
	HST-3-3	17	2.95	30.3	30.1	74.9	5.17	0.74	22.6	6.40	1.57	0.84	4.00	0.79
	HST-3-4	18	2.30	29.7	50.2	nd	nd	nd	nd	5.39	2.62	0.22	2.55	nd
	HST-3B-Av	103	1.81	29.0	29.7	78.5	5.53	0.73	26.1	6.07	1.76	0.33	3.99	0.84
Average	GC-3	101	1.41	21.9	20.8	84.1	5.26	0.76	27.2	6.79	0.38	0.53	5.87	1.37
	HST-3	84	1.85	29.4	27.3	79.2	5.78	0.73	26.0	6.15	1.61	0.35	4.20	0.85
	All		1.58	25.1	23.1	82.3	5.48	0.74	26.8	6.51	0.86	0.46	5.19	0.96

M moisture, *V* volatile matter, *A* ash yield, *C* carbon, *H* hydrogen, *N* nitrogen, $Q_{gr,ad}$ gross calorific value, on air-dried basis, S_t total sulfur, S_s sulfate sulfur, S_p sulfide sulfur, S_o organic sulfur, *ad* air-dry basis, *d* dry basis, *daf* dry and ash-free basis, R_r vitrinite random reflectance (%), *3B-Av* weighted average of the bench sample of the M3 seam (weighted by thickness of sample interval), *C* channel, *nd* not detected, *GC-3* average of M3 seam in Guanchong Mine, *HST-3* average of M3 seam in Heishentian Mine, *GC* Guanchong Mine, *LHD* Laoheidong Mine, *HST* Heishentian Mine

Proximate analysis, covering the determination of moisture, volatile matter, and ash yield, was conducted using American Society for Testing and Materials (ASTM) Standards D3173-11 (2011), D3175-11 (2011), and D3174-11 (2011). Total sulfur and forms of sulfur were determined following ASTM Standards D3177-02 (2002) and D2492-02 (2002), respectively. Samples were prepared for microscopic analysis in reflected light following ASTM Standard D2797/D2797M-11a (2011). Mean random reflectance of vitrinite (percent R_r) was determined using a Leica DM-4500P microscope (at a magnification of × 500) equipped with a Craic QDI 302™ spectrophotometer.

Concentrations of major element oxides in the samples (on an ash basis; 815 °C ashing temperature) were determined by X-ray fluorescence spectrometry. Mercury was determined using a Milestone DMA-80 Hg analyzer. Fluorine was determined by pyrohydrolysis with an ion-selective electrode, following the methods described in ASTM Standard D5987-96 (2002). Inductively coupled plasma mass spectrometry (ICP-MS) was used to determine other trace elements in the coal and rock samples. For ICP-MS analysis, the samples were digested using an UltraClave Microwave High Pressure Reactor. More details for these coal-related sample digestion and ICP-MS analysis techniques are given by Dai et al. (2013a, b). In order to significantly reduce argon-based interference at mass to charge ratios (*m*/*z*) 75 ($^{40}Ar^{35}Cl$) and 78 ($^{40}Ar^{38}Ar$), arsenic and Se were determined by collision/reaction cell technology (CCT) ICP-MS, based on the method outlined by (Li et al. 2014b). For boron determination by ICP-MS, addition of H_3PO_4 to the HNO_3 and HF was used to reduce boron volatilization during the acid-drying process after sample digestion, and 2 % ammonia was used as rinse solution to eliminate the memory effect of boron.

Low-temperature (oxygen-plasma) ashing (Gluskoter 1965) was carried out to remove the organic matter from the coal, using an EMITECH K1050X plasma asher. The low-temperature ash (LTA) residues of this process, and also the (untreated) non-coal rock samples, were analyzed by X-ray diffraction (XRD) using a D/max-2500/PC powder diffractometer with Ni-filtered Cu-$K\alpha$ radiation and a scintillation detector. The XRD patterns were recorded over a 2θ interval of 2.6 to 70°, with a step size of 0.01°. X-ray diffractograms were interpreted using the Siroquant software system (Taylor 1991), based on the principles developed by Rietveld (1969). Background was removed, a calibration function

applied to allow for the geometry of the diffraction system, and a synthetic XRD trace produced for each sample based on the minerals present. The structure of each phase making up the synthetic pattern was interactively refined until the best possible fit had been obtained between the synthetic pattern and the observed XRD trace, and the percentages of each phase indicated by the software recorded as a fraction of the sample concerned.

As well as the LTA residues, samples of the raw (i.e., unashed) coals were also analyzed by the same XRD techniques. The broad diffraction "hump" produced by the organic matter in these samples was removed (cf. Ward et al. 2001), so that the mineral percentages determined for those samples represent proportions of the total crystalline material in the coal concerned. Differences between the diffractograms for the raw coal and LTA of the same sample were used to identify any changes in the mineral matter induced by the low-temperature ashing process.

The chemical composition of the (high-temperature) coal ash expected to be derived from the mineral assemblage indicated by the XRD and Siroquant analyses of each coal or rock sample was calculated, using methodology described by (Ward et al. 1999). This process included calculations to allow for the loss of hydroxyl water from the clay minerals and CO_2 from the carbonates, at the temperatures associated with high-temperature (815 °C) ashing and combustion processes. Chemical data for the samples were recalculated to provide normalized percentages of the major element oxides in the inorganic fraction (loss-on-ignition free basis). These were taken to represent the chemical composition of the (high-temperature) ash derived from each sample. The inferred percentages of major element oxides in the coals and partings, as calculated from the XRD data, were then compared to the normalized percentages of the same oxides in the SO_3-free ash as calculated from the geochemical data obtained by separate XRF analysis.

A Field Emission-Scanning Electron Microscope (FE-SEM, FEI Quanta^{TM} 650 FEG), in conjunction with an EDAX energy dispersive X-ray spectrometer (Genesis Apex 4), was used to study morphology and microstructure, and also to determine the distribution of some elements in the coal and rock samples. Samples were made into pellets, polished, coated with carbon using a Quorum Q150T ES sputtering coater, and then mounted on standard aluminum SEM stubs using sticky electron-conductive carbon tabs. The working distance of the FE-SEM-EDS was 10 mm, beam voltage 20.0 kV, aperture 6, and spot size 5–6. Images were captured via a retractable solid state backscatter electron detector or a secondary electron detector.

Results

Coal chemistry and vitrinite reflectance

The vitrinite random reflectance (R_r) and volatile matter yields (V_{daf}, dry and ash-free basis) (Table 1) indicate that the rank of the Guiding coals varies from high (HST-3), through medium (LHD-1), to low volatile bituminous (GC-1 and GC-3), according to the ASTM classification (ASTM Standard D388–12 2012). Due to the presence of high calcite percentages in the coal, bench samples GC-3-1, GC-3-2, and GC-3C have higher volatile matter yields than the other coal benches (GC-3-3 and GC-3-4).

For comparison, the coals from Yanshan (R_r=1.81 %; Dai et al. 2008), Heshan (R_r=1.74–1.92 %; Dai et al. 2013a; Shao et al. 2003), and Fusui (R_r=1.41-1.56 %; Dai et al. 2013b) are all low volatile bituminous in rank. The average volatile matter yield of the Chenxi coals, however, is 42.11 % (Li and Tang 2013; Li et al. 2013), indicating a high volatile bituminous rank.

The Guiding coals have high organic sulfur contents, varying from 2.42 to 6.62 %, with an average of 5.19 %, but are characteristically low in pyritic sulfur (0.10–3.15 %; 0.86 % on average). These coals are classified as SHOS coals. In addition to the above-mentioned Late Permian SHOS coals of southern China, SHOS coals have also been reported from other areas, e.g., coals of Tertiary age along the on-shore margin of the Gippsland Basin, Victoria, Australia (Smith and Batts 1974); the Permian Tangorin coal seam of the Cranky Corner Basin, eastern Australia (Marshall and Draycott 1954; Ward et al. 2007); and the Upper Palaeocene Raša coal from Istria (Slovenia), which contains up to 11 % organic sulfur (Damste et al. 1999).

The Guiding coals are classified as medium-ash coals according to Chinese Standard GB/T 15224.1-2004 (2004); coals with ash yields of 16.01 to 29 % are medium-ash coals and those with ash >29.00 % are high-ash coals.

Major and trace elements

Table 2 lists the concentrations of major element oxides and trace elements in the samples from the Guiding Coalfield. Compared to average values for Chinese coals (Table 2; Dai et al. 2012b), K_2O and MgO, and to a lesser extent, SiO_2, are enriched in the Guiding coal. The remaining major element oxides are either lower than or close to the average values for Chinese coals (Table 2; Dai et al. 2012b).

Trace elements in the four different coal seams show similar abundances (Table 2; Fig. 3). Compared to average values for world hard coals (Ketris and Yudovich 2009), uranium, Re, and Mo are unusually enriched in the Guiding coals, with a concentration coefficient >100 (CC = ratio of element concentration in investigated coals vs. world hard coals); elements

Table 2 Major element oxides (%) and trace elements (μg/g) in the coal samples of the Guiding Coalfield (on a coal basis). GC, Guanchong Mine. LHD, Laoheidong Mine. HST, Heishentian Mine

Sample No. & Type		SiO_2	TiO_2	Al_2O_3	Fe_2O_3	MgO	CaO	Na_2O	K_2O	SiO_2/Al_2O_3	LOI	Li	Be	B	F	P	Cl	Sc	V	Cr	Mn	Co	Ni	Cu	Zn
GC-1C	Channel	10.2	0.21	5.33	1.68	0.52	1.82	0.087	0.93	1.91	76.7	29.1	1.11	47.9	1915	33.9	1329	3.62	1153	461	33.5	5.02	134	45.3	98.1
LHD-1C	Channel	7.20	0.18	3.48	1.34	0.49	1.53	0.030	0.74	2.07	83.1	18.5	1.34	22.7	1725	33.0	821	2.77	835	246	20.3	3.83	88.8	38.8	36.7
GC-3C	Channel	11.0	0.26	5.32	1.50	0.62	1.80	0.041	1.06	2.07	76.2	25	1.21	41.2	2118	41.2	1016	4.08	1013	548	22.5	3.07	110	43.0	60.3
GC-3-1	Bench	20.0	0.50	9.28	1.96	1.10	6.79	0.060	1.93	2.16	51.8	27.5	1.13	60.0	2554	56.5	725	6.91	1388	1094	42.6	5.91	221	69.8	62.6
GC-3-2	Bench	8.60	0.18	4.14	1.10	0.53	2.56	0.032	0.81	2.08	79	20.4	0.97	35.6	1768	28.4	1396	3.20	1127	677	22.0	4.76	175	44.8	75.1
GC-3-3	Bench	6.99	0.17	3.60	1.24	0.41	0.78	0.029	0.73	1.94	84.9	20.8	1.18	34.6	1623	26.3	1057	3.21	938	360	9.94	1.26	52.1	25.3	44.6
GC-3-4	Bench	7.44	0.18	3.86	1.31	0.44	0.87	0.028	0.77	1.93	83.7	22.8	1.24	36.9	1296	28.5	1064	3.37	805	366	12.5	1.92	57.6	32.7	61.0
GC-3-5	Bench	6.17	0.18	3.22	1.58	0.34	0.81	0.024	0.64	1.92	86.1	20.2	1.22	30.0	1590	38.8	1266	3.56	479	204	12.9	1.28	35.1	25.1	38.1
GC-3B-Av	Average	7.75	0.19	3.90	1.38	0.45	1.46	0.030	0.78	1.99	82.3	21.2	1.16	34.9	1621	33.1	1184	3.55	808	405	15.5	2.32	79.8	32.8	52.5
HST-3C	Channel	12.0	0.44	5.63	2.40	0.74	0.20	0.032	1.11	2.13	76.5	27.3	1.56	41.8	2370	57.0	697	5.22	838	268	37.7	8.60	97.0	55.5	74.4
HST-3-0	Bench	20.6	1.29	11.0	4.70	1.19	0.39	0.136	2.18	1.87	56.7	40.0	1.60	nd	3575	60.1	1131	10.2	770	583	97.9	10.4	123	72.1	92.8
HST-3-1	Bench	11.8	0.39	6.22	2.46	0.73	0.33	0.053	1.34	1.9	75.8	28.9	2.23	55.1	2429	30.6	629	4.89	1647	487	25.5	10.9	152	38.9	98.1
HST-3-2	Bench	7.32	0.17	3.50	1.41	0.44	0.12	0.030	0.74	2.09	85.8	15.9	1.30	27.4	1485	23.1	807	2.87	902	237	12.4	4.41	94.1	31.8	55.1
HST-3-3	Bench	15.3	0.64	6.95	3.34	0.91	0.21	0.029	1.30	2.2	69.9	32.6	1.56	49.3	2697	93.0	802	6.91	645	243	60.3	13.6	95.1	73.3	109
HST-3-4	Bench	31.1	0.93	8.90	4.33	1.05	0.27	0.050	1.67	3.49	49.8	42.7	1.74	78.6	3271	229	628	9.93	365	246	68.1	10.7	71.3	87.3	70.9
HST-3B-Av	Average	15.8	0.62	6.73	2.98	0.80	0.23	0.056	1.33	2.35	70.3	29.3	1.57	37.4	2495	78.5	821	6.38	812	331	47.9	8.82	102	56.9	78.3
All Guiding coals		11.1	0.34	5.21	1.94	0.62	1.11	0.040	1.03	2.13	76.9	25.3	1.33	37.9	2076	48.8	973	4.49	892	391	29.7	5.26	99.7	45.5	66.0
World or China*		8.47	0.33	5.98	4.85	0.22	1.23	0.16	0.19	1.42	nd	14	2.0	47	82	250	340	3.7	28	17	71	6.0	17	16	28

Sample No. & Type		Ga	Ge	As	Se	Rb	Sr	Zr	Nb	Mo	Cd	In	Sn	Sb	Cs	Ba	Ta	W	Re	Hg(ng/g)	Tl	Pb	Bi	Th	U
GC-1C	Channel	6.94	1.22	8.79	29.7	26.3	176	86.7	7.13	472	6.69	0.039	1.43	0.90	1.58	48.8	0.41	1.24	0.76	187	3.53	12.7	0.37	4.62	288
LHD-1C	Channel	5.27	0.73	18.3	14.2	20.3	143	44.1	4.90	419	3.10	0.023	0.60	0.81	3.01	44.9	0.35	0.67	0.14	76.6	2.39	6.63	0.18	1.91	229
GC-3C	Channel	6.10	1.09	6.62	42.6	36.3	210	67.6	6.78	349	3.28	0.040	0.86	1.03	2.02	76.4	0.51	1.42	0.54	175	3.41	9.43	0.32	3.03	211
GC-3-1	Bench	8.51	0.89	11.2	77.1	54.6	513	141	12.8	210	4.43	0.051	1.24	1.69	2.56	107	0.99	1.56	2.34	258	4.92	8.46	0.27	4.94	157
GC-3-2	Bench	4.67	0.89	6.90	29.9	25.6	204	67.8	5.80	362	4.16	0.035	0.68	0.92	1.47	59.9	0.36	0.93	0.98	146	2.76	6.98	0.20	2.32	273
GC-3-3	Bench	4.67	1.54	5.56	27.3	25.0	124	43.2	4.91	387	2.25	0.035	0.73	0.84	1.64	58.6	0.34	1.09	0.05	153	2.77	6.37	0.26	2.16	176
GC-3-4	Bench	5.05	1.35	5.32	29.6	27.2	146	48.2	5.49	398	2.50	0.048	0.76	0.78	1.72	64.3	0.36	0.67	0.09	179	2.60	8.00	0.26	2.50	193
GC-3-5	Bench	4.62	1.21	5.16	27.4	22.4	123	48.9	5.52	320	1.55	0.048	0.78	0.65	1.62	48.2	0.35	1.13	0.06	174	1.96	6.74	0.20	2.17	147
GC-3B-Av	Average	4.92	1.22	5.92	30.8	26.1	163	55.9	5.81	352	2.54	0.040	0.77	0.82	1.66	58.7	0.38	1.01	0.36	169	2.55	7.05	0.23	2.40	187
HST-3C	Channel	8.24	1.41	7.86	32.5	35.8	175	78.1	9.99	369	3.29	0.041	1.02	1.12	2.00	69.8	0.80	1.22	0.13	154	2.85	8.72	0.24	3.30	223
HST-3-0	Bench	12.0	0.94	33.6	100	58.0	199	166	25.9	232	4.37	0.080	1.37	2.58	2.88	84.9	1.81	1.95	0.12	359	3.74	14.0	0.31	6.53	95.3
HST-3-1	Bench	7.67	0.99	8.14	29.2	43.3	248	80.9	9.16	387	3.91	0.043	1.05	1.25	2.19	92.8	0.70	0.66	0.30	149	5.20	11.2	0.37	2.99	281
HST-3-2	Bench	5.66	2.07	4.24	13.9	23.3	171	41.3	5.13	430	2.85	0.022	0.69	0.84	1.19	45.5	0.36	0.59	0.07	83.0	2.89	6.64	0.18	2.15	269
HST-3-3	Bench	10.6	2.64	9.61	45.2	37.5	162	101	15.6	321	3.76	0.054	1.43	1.40	2.26	55.8	1.09	1.30	0.09	198	2.64	8.21	0.19	3.97	198
HST-3-4	Bench	12.6	0.75	12.1	57.1	45.4	255	143	21.0	174	2.96	0.066	1.42	1.77	2.58	186	1.57	1.52	0.06	218	1.98	11.0	0.23	4.44	67.9
HST-3B-Av	Average	9.11	1.61	12.6	44.8	38.2	197	97.0	14.0	325	3.42	0.048	1.11	1.47	2.04	84.0	1.01	1.14	0.10	185	3.08	9.53	0.23	3.78	190
All Guiding coals		6.83	1.26	9.24	35.3	32.1	182	72.8	8.55	364	3.43	0.041	0.95	1.07	1.99	68.0	0.61	1.15	0.32	165	2.98	8.86	0.26	3.14	211
World or China*		6.0	2.4	9.0	1.6	18	100	36	4.0	2.1	0.20	0.040	1.4	1.00	1.1	150	0.30	0.99	nd	0.10	0.58	9.0	1.1	3.2	1.9

3B-Av, weighted average for coal benches of M3 seam (weighted by thickness of sample interval); C, channel; All Guiding coals, the average concentration for all coals from the Guiding Coalfield. bdl, below detection limit. nd, no data. *, Average values of major-element oxides for Chinese coals and trace elements for world hard coals are from Dai et al. (2012b) and Ketris and Yudovich (2009), respectively.

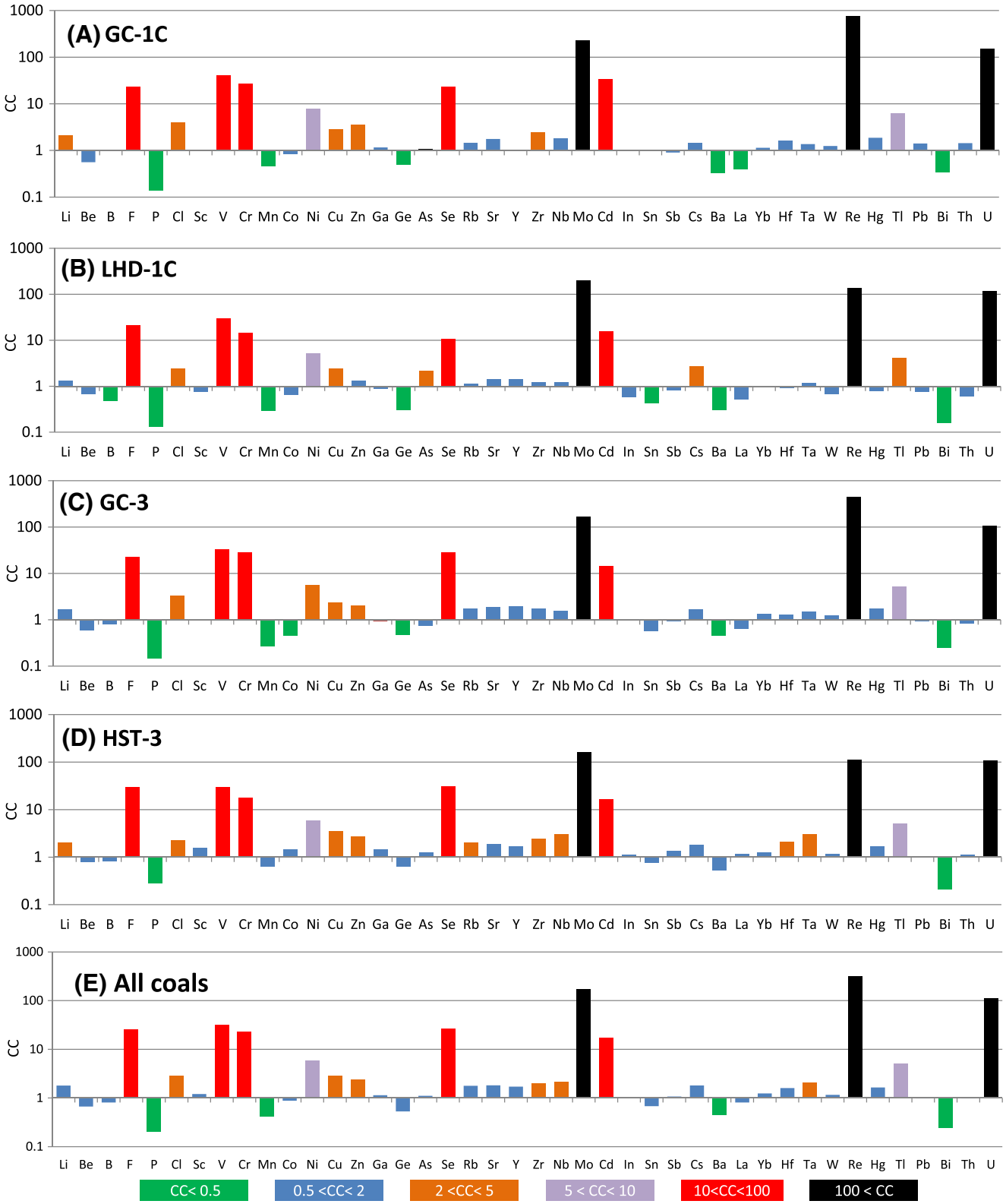

Fig. 3 Concentration coefficients (*CC*) of trace elements in the Guiding coals. Normalized to average trace-element concentrations in world hard coals (Ketris and Yudovich 2009)

such as F, V, Cr, Se, and Cd are significantly enriched (10 < CC < 100); Ni and Tl are enriched (5 < CC < 10); Cl, Cu, Zn, Zr, and in some cases, Nb and Ta are slightly enriched (2 < CC < 5). However, P, Mn, Ba, and Bi are depleted (CC < 0.5). The

remaining elements (0.5 < CC < 2) are close to the average values for world hard coals (Ketris and Yudovich 2009).

The B concentration in the Guiding coals (37.9 μg/g on average) is slightly lower than the average value for world hard coals (47 μg/g; Ketris and Yudovich 2009). It is not as high as might be expected when compared to the indices developed by Goodarzi and Swaine (1994), who placed the fresh/brackish and brackish/marine boundaries at 50 and 110 μg/g B, respectively. The B concentration in the Guiding coals is much lower than that in coals (>110 μg/g) reported to have formed under heavy marine influence (Goodarzi and Swaine 1994; Eskenazy et al. 1994; Chen et al. 2011).

Like the Guiding coals, the coals formed on restricted carbonate platforms in the Heshan (Dai et al. 2013a), Yanshan (Dai et al. 2008), and Chenxi (Li et al. 2013) coalfields have similar trace element (U, Se, Mo, Re, and V) enrichment assemblages (Fig. 4a–c). Although the coals of the Fusui Coalfield were formed on an open carbonate platform, as compared with the averages for world hard coals (Ketris and Yudovich 2009) they also have elevated concentrations of U, Se, and Mo, but not to the extent of those in the Guiding, Heshan, and Yanshan coals (Fig. 4d).

Rare earth elements and yttrium

Three enrichment types for REY are used in this study, based on the classification of Seredin and Dai (2012). The average concentration (weighted by thickness of sample interval) of total REY in both the channel and bench samples of the

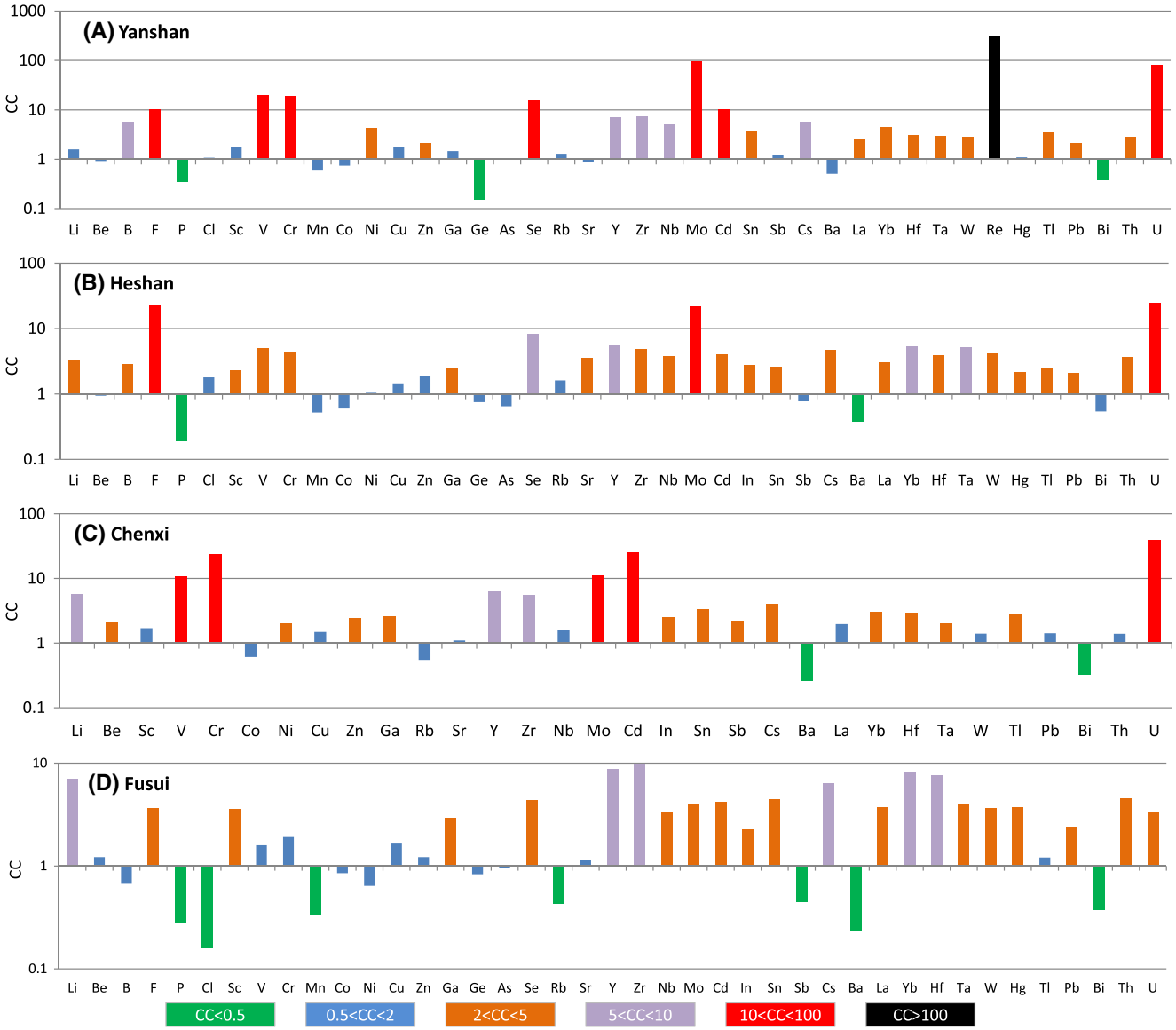

Fig. 4 Concentration coefficients (*CC*) of trace elements in the Yanshan (Dai et al. 2008), Heshan (Dai et al. 2013a), Chenxi (Li and Tang 2013; Li et al. 2013), and Fusui coals (Dai et al. 2013b). Normalized to average trace element concentrations in world hard coals (Ketris and Yudovich 2009)

Guiding coal is 63.6 μg/g (Table 3), which is close to the average value for world hard coals (68.6 μg/g; Ketris and Yudovich 2009). The REY enrichment in all the Guiding coals is characterized by the H-REY type ($La_N/Lu_N < 1$; Fig. 5), similar to those of coals from the Yanshan, Heshan, Fusui, and Chenxi coalfields (Fig. 6).

The REY distribution patterns in the Guiding coals are characterized by very weak Eu and Ce anomalies, either positive or negative (Fig. 5), similar to those of the Late Permian coals containing sediment derived from the basaltic Kangdian Upland regions (Dai et al. 2014a; Fig. 1a). However, the coals from the Yanshan, Heshan, and Fusui coalfields are characterized by weak Ce and distinct negative Eu anomalies; the Chenxi coals do not show an Eu anomaly (Fig. 6). Samples GC-3 and LHD-1C, and, to a lesser extent, HST-3, have a positive Y anomaly (Fig. 5a–d), similar to the Yanshan coals (Fig. 6). The GC-1C section does not show a distinct Y anomaly (Fig. 5d), similar to the Heshan and Fusui coals (Fig. 6).

The distinct negative Eu anomaly in the Yanshan, Heshan, and Fusui coals suggests that the terrigenous materials admixed with these coals were different from those found in most of the Late Permian coals of southwestern China (including the Guiding coals), whose sediment-source region was the basaltic Kangdian Upland (Fig. 1a). The sediment-source region for the Yanshan coals was the felsic rhyolite-dominated Northern Vietnam Upland (Fig. 1a; Li and Xu 2000; Chen et al. 2003), while the sediment source for the Heshan and Fusui coals was the Yunkai Upland (Fig. 1a), which formed at an early stage of the Late Permian and is mainly composed of felsic Permo-Carboniferous rocks (Feng et al. 1994).

Modes of occurrence of some trace elements in the Guiding coals

1. Uranium, Mo, V, and Re

   Uranium and Mo are negatively correlated with ash yield (Table 4; Fig. 7), indicating that U and Mo are mainly associated with the coals' organic matter. Additionally, a small proportion of U occurs in mineral form (e.g., coffinite and brannerite) as described below. The correlation coefficient between U and Mo is 0.85 (Table 4; Fig. 7), indicating that U and Mo have similar geochemical behavior in the coal.

   The correlation coefficient between V and ash yield is −0.05 (Fig. 7), indicating a mixture of both organic and inorganic modes of occurrence. As indicated by the correlation coefficient of V with jarosite ($r=0.45$), jarosite may be the mineral carrier for a proportion of the V in the coal.

   Seredin and Finkelman (2008) also showed that U in worldwide U-bearing coal deposits is mainly associated with organic matter, and that only a small

Table 3 Concentration of rare earth elements and yttrium in the coal samples from the Guiding Coalfield (μg/g; on a coal basis)

Sample no.	La	Ce	Pr	Nd	Sm	Eu	Gd	Tb	Dy	Y	Ho	Er	Tm	Yb	Lu	REY
GC-1C	4.39	8.82	1.13	4.96	1.21	0.25	1.25	0.23	1.54	8.07	0.33	1.13	0.18	1.2	0.19	34.9
LHD-1C	5.26	12.3	1.60	7.09	1.54	0.33	1.67	0.24	1.64	11.3	0.32	1.08	0.14	1.03	0.14	45.7
GC-3C	7.36	15.2	1.88	7.96	1.68	0.35	1.86	0.28	1.99	15.2	0.42	1.45	0.20	1.43	0.21	57.5
GC-3-1	10.6	20.5	2.40	9.73	1.72	0.34	1.8	0.25	1.75	13.4	0.37	1.35	0.19	1.41	0.21	66.0
GC-3-2	4.04	8.35	1.08	4.83	1.13	0.24	1.27	0.21	1.56	12.6	0.35	1.26	0.18	1.31	0.19	38.6
GC-3-3	5.52	12.1	1.55	6.93	1.53	0.33	1.72	0.26	1.93	14.7	0.40	1.40	0.19	1.38	0.20	50.1
GC-3-4	6.95	14.8	1.83	7.93	1.71	0.36	1.91	0.28	1.99	15.9	0.40	1.38	0.18	1.30	0.18	57.1
GC-3-5	6.57	12.6	1.63	7.22	1.64	0.35	1.85	0.28	2.07	14.5	0.43	1.48	0.20	1.48	0.21	52.5
GC-3B-Av	6.48	13.6	1.59	6.73	1.40	0.3	1.65	0.25	1.80	15.4	0.39	1.30	0.18	1.29	0.22	52.6
HST-3C	10.7	24.5	2.90	12.4	2.47	0.54	2.56	0.34	2.22	13.5	0.42	1.37	0.18	1.27	0.18	75.6
HST-3-0	15.1	27.4	2.91	11.2	1.86	0.37	1.96	0.27	1.87	9.93	0.37	1.30	0.19	1.40	0.20	76.3
HST-3-1	6.93	14.8	1.70	7.22	1.58	0.36	1.74	0.26	1.80	11.0	0.36	1.20	0.17	1.21	0.17	50.5
HST-3-2	6.66	16.1	1.96	8.59	1.80	0.38	1.92	0.26	1.69	11.9	0.33	1.07	0.13	0.97	0.13	53.9
HST-3-3	14.1	31.6	3.75	16.1	3.23	0.72	3.24	0.43	2.76	15.5	0.51	1.62	0.21	1.48	0.20	95.5
HST-3-4	18.8	46.1	4.92	21.0	4.13	0.94	3.99	0.5	3.06	14.1	0.56	1.78	0.23	1.66	0.22	122
HST-3B-Av	13.8	29.6	3.24	13.3	2.43	0.55	2.59	0.35	2.19	14.0	0.43	1.35	0.18	1.28	0.21	85.6
All Guiding coals	8.94	19.4	2.18	9.07	1.77	0.38	1.98	0.28	1.90	14.4	0.40	1.28	0.17	1.24	0.21	63.6
World[a]	11	23	3.4	12	2.2	0.43	2.7	0.31	2.1	8.2	0.57	1.00	0.30	1.0	0.20	68.6

3B-Av weighted average for coal benches of M3 seam (weighted by thickness of sample interval), *C* channel, *All Guiding coals* the average concentration for all coals from Guiding Coalfield

[a] World hard coals, data from Ketris and Yudovich (2009)

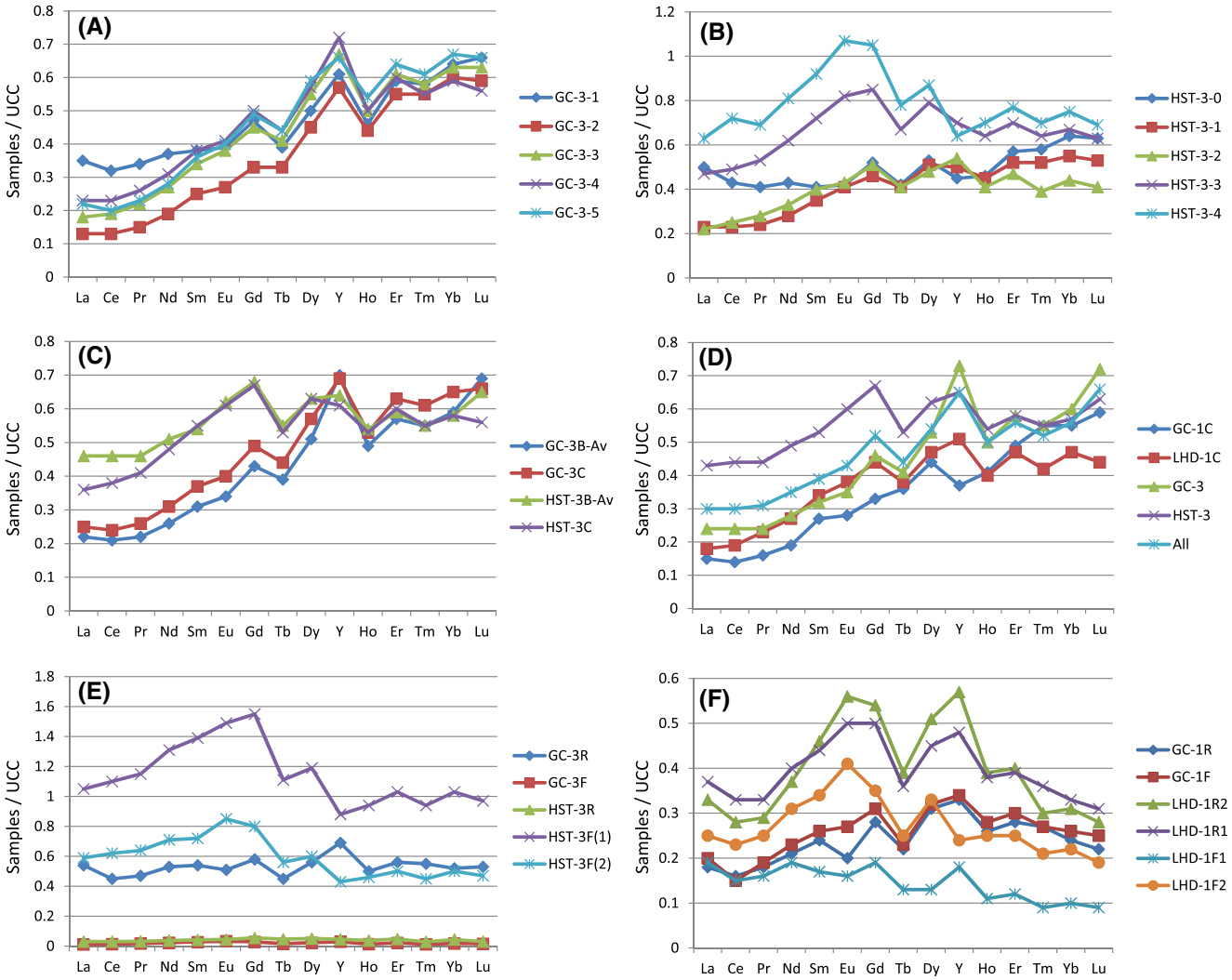

Fig. 5 REY distribution patterns of Guiding coals (on a coal basis) and host rocks. **a** Coal benches of M3 seam in the Guanchong Mine. **b** Coal benches of M3 seam in the Heishentian Mine. **c** Bench average and channel sample of M3 seam from the Guanchong and Heishentian Mines. **d** Channel samples of M1 seam and average of M3 seam. **e**, **f** Roof and floor strata samples. REY are normalized to the Upper Continental Crust (*UCC*) (Taylor and McLennan 1985). *R*, roof; *F*, floor

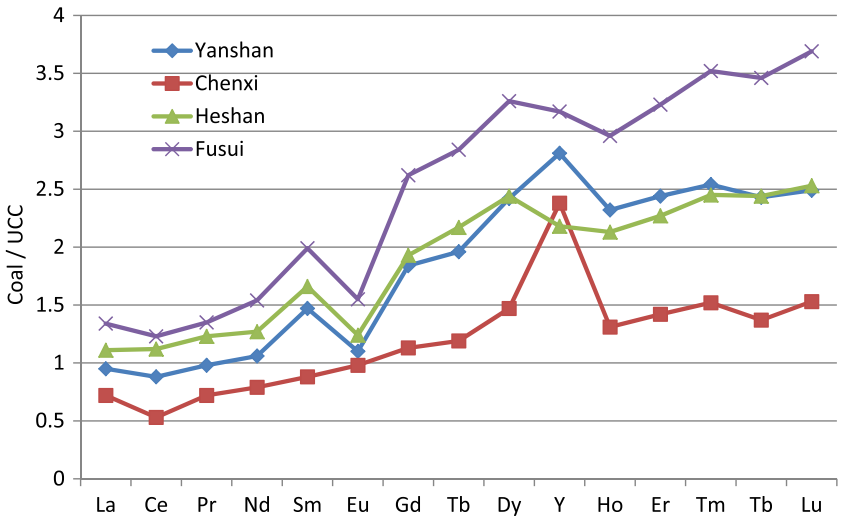

Fig. 6 REY distribution patterns of Late Permian coals from the Yanshan, Heshan, Fusui, and Chenxi coalfields (on a coal basis). REY are normalized to the Upper Continental Crust (*UCC*) (Taylor and McLennan 1985)

Table 4 Element affinities deduced from the calculation of Pearson correlation coefficients between the concentrations of each element in coal and ash yield or selected major elements

Correlation with ash yield
r_{ash}=0.7–1.0
S_p (0.80), SiO_2 (0.95), TiO_2 (0.82), Al_2O_3 (0.95), Fe_2O_3 (0.77), MgO (0.95), K_2O (0.93), Li (0.84),
B (0.90), F (0.88), P (0.70), Sc (0.91), Mn (0.83), Cu (0.92), Ga (0.86), Se (0.86), Rb (0.89),
Sr (0.71), Zr (0.96), Nb (0.86), In (0.76), Sn (0.77), Sb (0.87), Ba (0.80), Hf (0.94), Ta (0.88),
W (0.76), Hg (0.75), Th (0.84), REY (0.76)
r_{ash}=0.40-0.69
Na_2O (0.57), Cr (0.48), Co (0.62), Ni (0.45), Zn (0.40), As (0.53), Cs (0.64), Re (0.42), Pb (0.58)
r_{ash}: from −0.29 to 0.35
CaO (0.35), Be (0.30), Y (0.27), Tl (0.32), Bi (0.21), Cd (0.35), V (−0.05)
r_{ash}: from −1.0 to −0.3
S_t (−0.86), S_o (−0.91), Cl (−0.37), Ge (−0.30), Mo (−0.86), U (−0.63)
Correlation coefficients between selected pairs of elements
U-Mo=0.85
F-B=0.88, F-Na_2O=0.65, F-MgO=0.94, F-Al_2O_3=0.94, F-SiO_2=0.88, F-K_2O=0.92,
F-Mn=0.94, F-Fe_2O_3=0.94, F-Cr=0.22
M_{ad}-Cl=−0.22, Cl-Na_2O=0.17, Cl-Al_2O_3=−0.32, Cl-SiO_2=−0.45, B-MgO=0.88; B-K_2O=0.85

proportion usually occurs in the minerals. However, the mode of occurrence of Mo in the present study is different from that described by Seredin and Finkelman (2008), who showed that Mo mainly occurs as molybdenite in U-bearing coal deposits. A combination of SEM-EDX analysis and sequential solvent extraction by Dai et al. (2008) showed that U, Mo, and V, as well as Cr and Ni, in the Yanshan SHOS coal occur not only in silicate minerals but also in the organic matter.

Rhenium is positively correlated with ash yield (r=0.42), suggesting an inorganic association in the Guiding coals. Rhenium is positively correlated with jarosite (r=0.56) and calcite (r=0.92) (Fig. 7), indicating that Re probably occurs in secondary sulfates (derived from sulfide oxidation) and carbonate minerals. Since the concentration of Re is usually very low in coal (<0.001 μg/g; Finkelman 1993), it is difficult to directly identify Re-bearing minerals in coal samples. However, Yossifova (2014) identified Re-bearing inorganic phases in the dry residues obtained from water leachates derived from coal slurries and raw coals, possibly representing oxides and/or hydroxides, altered sulfides, carbonates, and chlorides. These Re-bearing phases were either originally present in the coal or were the altered/neoformed products during oxidation and dehydration process (Yossifova 2014).

2. Selenium, Hg, As, Tl, and Cd

Selenium, Hg, and As are all positively correlated with ash yield (Table 4), having correlation coefficients of

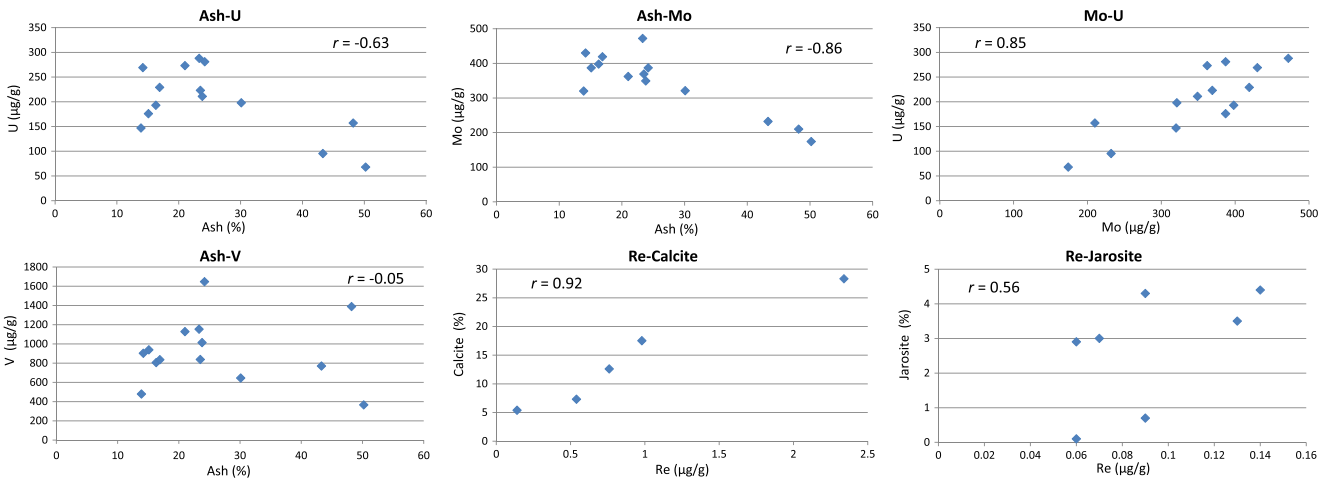

Fig. 7 Relation of ash yield-U, ash yield-Mo, Mo-U, ash yield-V, Re-calcite, and Re-jarosite

0.86, 0.75, and 0.53, respectively; these indicate mainly inorganic associations. In addition, Se, Hg, and As are positively correlated with pyrite, having correlation coefficients of 0.71, 0.75, and 0.89, respectively; however, these three elements are negatively correlated with marcasite (correlation coefficients of −0.82, −0.76, and −0.71, respectively; Fig. 8), suggesting that Se, Hg, and As mainly occur in pyrite rather than in marcasite. Selenium in the Fusui coals is mainly distributed in marcasite, although both pyrite and marcasite occur as contemporaneous phases in the same coal (Dai et al. 2013b).

A number of modes of Se occurrence have been identified in high-Se coals; these include native Se, ferroselite ($FeSe_2$), sulfide minerals containing Se as an isomorphic admixture (pyrite, arsenopyrite, chalcopyrite, galena, etc.) (Maksimova and Shmariovich 1993; Kislyakov and Shchetochkin 2000; Fu et al. 2013), and clausthalite (Finkelman 1980; Hower and Robertson 2003). A portion of the Se may also occur in the organic matter of high-Se coals (Yudovich and Ketris 2005).

Thallium is positively correlated with marcasite (r= 0.86) but weakly correlated with pyrite (r=−0.09), suggesting an association with marcasite. The correlation coefficients for Cd-illite, Cd-illite/smectite (I/S), and Cd-illite + I/S are −0.07, 0.56, and −0.12, respectively, and those of Cd-Mg, Cd-Na, and Cd-K are 0.35, 0.63, and 0.37, respectively, suggesting that Cd is mainly associated with mixed-layer illite/smectite rather than illite.

3. Fluorine and Cl

Previous studies have shown that fluorine in coal generally occurs in minerals such as clays and fluorapatite, and less commonly in tourmaline, topaz, amphiboles, and micas (Finkelman 1995; Godbeer and Swaine 1987; Swaine 1990); in addition, fluorine may also have an organic affinity (Bouška et al. 2000; McIntyre et al. 1985; Wang et al. 2011). The high concentration of F (up to 3362 μg/g) in the Heshan coals mainly occurs in epigenetic fluorite, and a very small proportion of F- and REY-bearing $CaMgCO_3$(F) was also detected in those coals (Dai et al. 2013b).

The correlation coefficient between fluorine and ash is high (r=0.88; Fig. 9), suggesting an inorganic association. Moreover, the positive correlation coefficients between F and several other components, including B, Na_2O, MgO, Al_2O_3, SiO_2, K_2O, CaO, V, Mn, Fe_2O_3, and Cr (Table 4), suggests that the F in the Guiding coals probably occurs in tourmaline that is mainly composed of the above F-positively correlated components. However, tourmaline was not observed by XRD or by SEM-EDS and optical microscopy due to its low concentration in the coal.

The Cl in coal has been extensively investigated (Skipsey 1975; Daybell and Pringle 1958; Caswell 1981; Caswell et al. 1984; Hower et al. 1991; Huggins and Huffman 1995; Ward et al. 1999; Vassilev et al. 2000; Spears 2005) and some possible modes of occurrence have been proposed, for example, as organic compounds, as impurity components in the crystalline and amorphous inorganic constituents, as discrete minerals (Vassilev et al. 2000), and associated with the coal moisture (Spears 2005). However, as discussed by Dai et al. (2012a), it is not possible for Cl to occur as organic phases and as HCl, based on the molecular (Cl_2) free radical reaction mechanism (Liang, 2001). In the present study, the mode of occurrence of Cl as NaCl is also discounted because of the low correlation coefficient between Na_2O and Cl (0.17; Table 4).

With the exception of organic sulfur, almost all the elements are weakly or negatively correlated with Cl. The low correlation coefficients for Cl-Al_2O_3 (r=−0.32), Cl-SiO_2 (r=−0.45), and Cl-K_2O (r=−0.37) indicate that Cl does not occur in the clay minerals (kaolinite, illite,

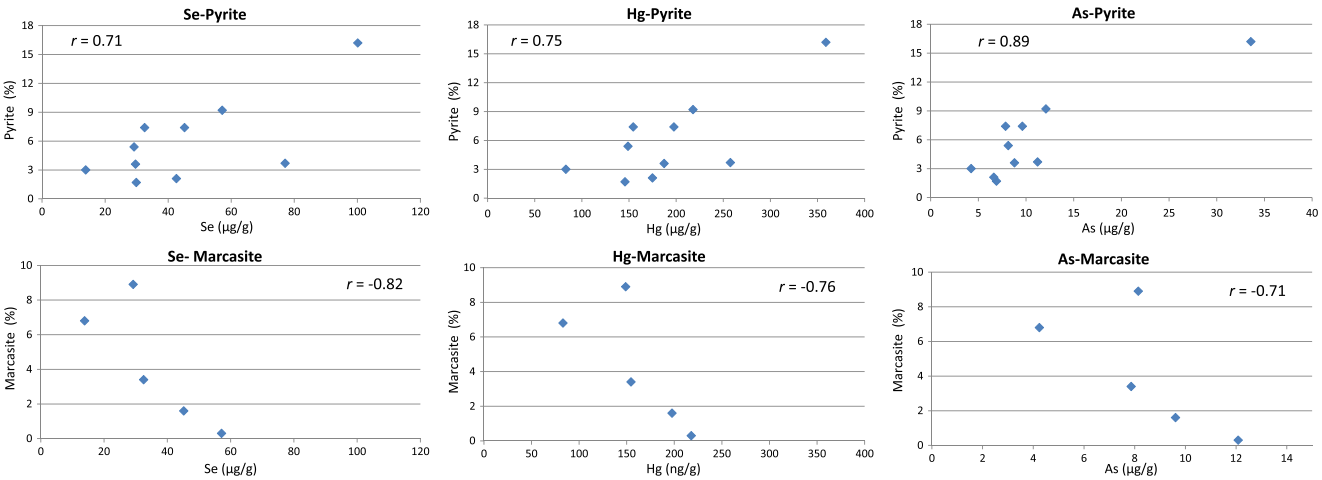

Fig. 8 Relation of Se to pyrite, Hg to pyrite, As to pyrite, Se to marcasite, Hg to marcasite, and Se to marcasite

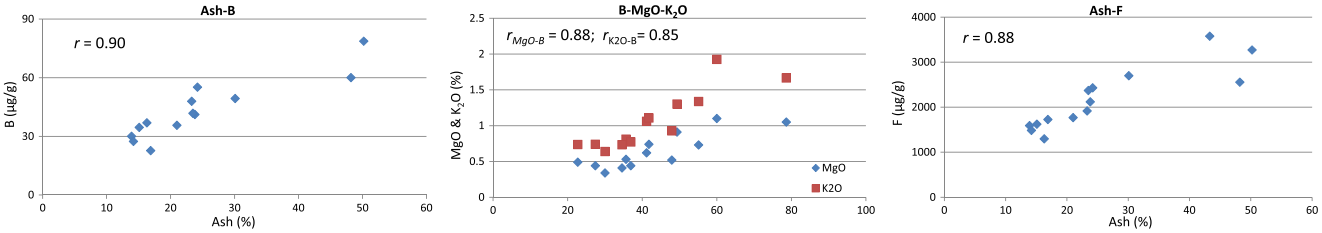

Fig. 9 Relation of ash yield to B, B to MgO, B to K_2O, and ash yield to F

mixed-layer I/S). It seems that Cl is unrelated to any other element groups in the coal. In addition, the correlation coefficient between Cl and moisture content is −0.22, indicating that Cl is not moisture-associated. Thus, it is reasonable that Cl could be adsorbed as Cl^- ions on to the coal's organic matter in the Guiding coals. The same mode of Cl occurrence was observed in the coals of the Gunnedah Basin, Australia (Ward et al. 1999).

4. Boron

Although the concentration of B is low in the Guiding coals (Table 2), the investigation of B in coal is significant because it is considered as a good paleosalinity indicator for the coal-forming environment (Goodarzi and Swaine 1994). Three modes of occurrence of B in coal are commonly recognized: bound to the organic matter, associated with some of the clay minerals (mainly illite), and bound within the crystal lattice of tourmaline (Ward 1980; Eskenazy et al. 1994; Finkelman 1995; Querol et al. 1995, 1999; Boyd 2002; Oliveira et al. 2013). Although illite and tourmaline may be locally important modes of occurrence, the organically bound mode is generally considered to be the most common (Ward 1980; Swaine 1990; Boyd 2002; Riley et al. 2012; Li et al. 2014a, b).

Boron in the present study is positively correlated with ash yield (r=0.90; Fig. 9), K_2O (r=0.88), MgO (r=0.85), mixed-layer I/S (r=0.55), and F (r=0.88; F mainly occurs in tourmaline as mentioned above), but negatively correlated with illite (r=−0.41), possibly indicating that the B is mainly associated with mixed-layer I/S and tourmaline rather than illite or organic matter. Because of its low concentration and its association with mixed-layer I/S and tourmaline, the B in the Guiding coals is thought to be of terrigenous region, rather than a derivation from marine or hydrothermal processes. Finkelman (1982) and Ren et al. (2006) have indicated that B of terrigenous origin is mainly associated with clay minerals.

Minerals present in coal and non-coal strata

The mineral percentages in the LTAs of the coal samples and in the non-coal rocks (roof and floor strata) are presented in Table 5 and the Electronic Supplementary File, respectively. Similar data, based on the crystalline fractions for the raw coals, are given in Table 6.

Table 5 Mineralogical compositions of coal LTA samples by XRD and Siroquant (wt%)

Sample	LTA	Quartz	Kaolinite	Illite	I/S	Calcite	Dolomite	Bassanite	Anhydrite	Pyrite	Marcasite	Jarosite
GC-1C	27.0	3.9	4.9	66.0		18.3		0.0	1.4	3.7		
GC-3-1	52.0	7.1		56.3		31.2			1.4	3.1		
GC-3-2	24.9	4.2		66.7		21.2	0.8	3.0	2.8	1.4		
GC-3-3	16.5	1.5	2.2	83.3				3.7	9.3			
GC-3-4	30.7	2.8	3.8	78.1				4.6	10.7			
GC-3-5	22.3	2.2	6.2	75.3				3.1	11.7			1.5
GC-3C	30.6	4.0	2.5	73.4		9.3		3.9	5.7	1.2		
HST-3-0	54.3	2.5	3.0	80.8				0.1	1.7	11.9		
HST-3-1	35.7	0.8	5.8	81.6				0.3	0.3	4.9	6.4	
HST-3-2	19.3	3.9	4.8	82.9					0.5	2.2	4.6	1.0
HST-3-3	50.7	7.3	6.1	77.9				0.1	1.4	6.2		1.0
HST-3-4	65.5	28.2	1.8	22.4	36.3			0.2	1.2	9.6	0.4	
HST-3C	38.9	3.8	4.8	80.6				0.1	1.4	5.6	2.4	1.3
LHD-1C	18.4	3.9	9.5	61.2		11.9	0.8	6.4	5.2			1.1

I/S mixed-layer illite/smectite

Table 6 Mineralogical compositions of crystalline fraction in raw coal samples by XRD and Siroquant (wt%)

Sample	Quartz	Kaolinite	Illite	I/S	Calcite	Gypsum	Pyrite	Marcasite	Jarosite	Anatase
GC-1C	5.7	4.8	67.7		12.6	5.6	3.6			
GC-3-1	9.4	1.4	54.9		28.3	2.1	3.7			0.2
GC-3-2	11.2	2.6	55.8		17.5	11.2	1.7			
GC-3-3	0.9	4.5	75.5			19.1				
GC-3-4	2.4	1.6	74.5			20.8			0.7	
GC-3-5	2.1	2.9	68.1			24.0			2.9	
GC-3C	6.1	1.8	67.0		7.3	15.7	2.1			
HST-3-1	1.3	3.2	32.0	48.8		0.5	5.4	8.9		
HST-3-2	5.8	9.5	44.1	26.0		1.7	3.0	6.8	3.0	
HST-3-3	10.2	3.4	17.2	52.5		2.4	7.4	1.6	4.3	0.9
HST-3C	5.9	3.1	30.3	42.7		3.7	7.4	3.4	3.5	
LHD-1C	7.8	6.4	30.5	31.0	5.4	14.5			4.4	

C channel sample, *I/S* mixed-layer illite/smectite

With the exception of the HST-3 floor samples, HST-3 F(1) and HST-3 F(2), the samples of the roof and floor strata are dominated by calcite, or, in some instances, dominated by quartz (e.g., GC-3 F, HST-3R2, and LHD-1 F1), further indicating that the roof and the roof strata are limestones or siliceous rocks. A trace of dolomite also occurs in some of the calcite-rich host rocks and coal LTAs.

The mineral matter in the LTA of most of the coal samples, however, is dominated by illite, with significant proportions of calcite, pyrite, and/or marcasite in some samples. Small proportions of bassanite and/or anhydrite are also present in most of the LTA residues.

The illite in the LTAs of the coals, and also in the raw coal of the GC seams, has a single XRD peak at around 10.3 Å. The illite in the raw coals from the HST and LHD mines, and also in the LTA of the HST floor samples, however, also has a second broad XRD peak at approximately 10.9 Å, which is taken to represent a separate I/S phase. The apparent absence of I/S from the LTA residues, despite its presence in the raw coals derived from the same samples, may reflect removal of interlayer water and collapse of the I/S with heating during the low-temperature ashing process.

Pyrite is present as a minor component in the mineral matter of the GC and LHD coals. However, it is abundant, along in some cases with marcasite, in the HST coal samples (e.g., HST-3-1, HST-3-2, and HST-3C), as well as in the HST floor materials. Jarosite, which is probably an oxidation product of pyrite and/or marcasite, is also present in some of the samples, especially the pyrite-rich materials from the HST mine.

Gypsum is present in most of the raw coals, especially in the GC-3 and LHD-1 samples (Table 6). The LTAs of the same samples, however, contain anhydrite, and in some cases bassanite, rather than gypsum. Although bassanite is commonly regarded as an artefact of plasma ashing, derived from interaction between organically associated Ca and S during maceral oxidation (Frazer and Belcher 1973), the bassanite and anhydrite in this instance at least partly represent dehydration products of gypsum already present in the coal samples from the study area.

A small proportion (4.6 %) of feldspar occurs in HST floor sample HST-3 F(2) (see Electronic Supplementary File). The XRD pattern of this material suggests that it has an albite structure. The normalized chemical analysis data for this particular sample also has the highest proportion of Na_2O in the sample series, consistent with the albite identification.

Comparison between chemical and XRD data

The relationship of the percentages of major element oxides (SO_3-free basis) inferred from the XRD analysis to the percentages of the same oxides (normalised, SO_3-free) derived from direct chemical analysis data are indicated in Fig. 10. The comparative data are presented as X-Y plots, with a diagonal line on each plot indicating where the points would fall if the estimates from the two different techniques were equal. The points for SiO_2 and CaO plot close to the equality line, suggesting that the inferred percentages of these elements from the XRD results are generally compatible with the chemical analysis data.

The points for Al_2O_3 lie close to the equality line at low concentrations, but at high concentrations the XRD indicates higher percentages of Al_2O_3 than those observed from the chemical analysis data. By contrast, while many of the points for Fe_2O_3 plot close to the equality line, a number of points fall well below that line, indicating an underestimation of Fe_2O_3 from the XRD data. This may in part reflect replacement of Al by Fe in the illite and interstratified I/S of the coal samples, which was not allowed for in calculating the inferred ash chemistry from the XRD data. A plot showing the relationship

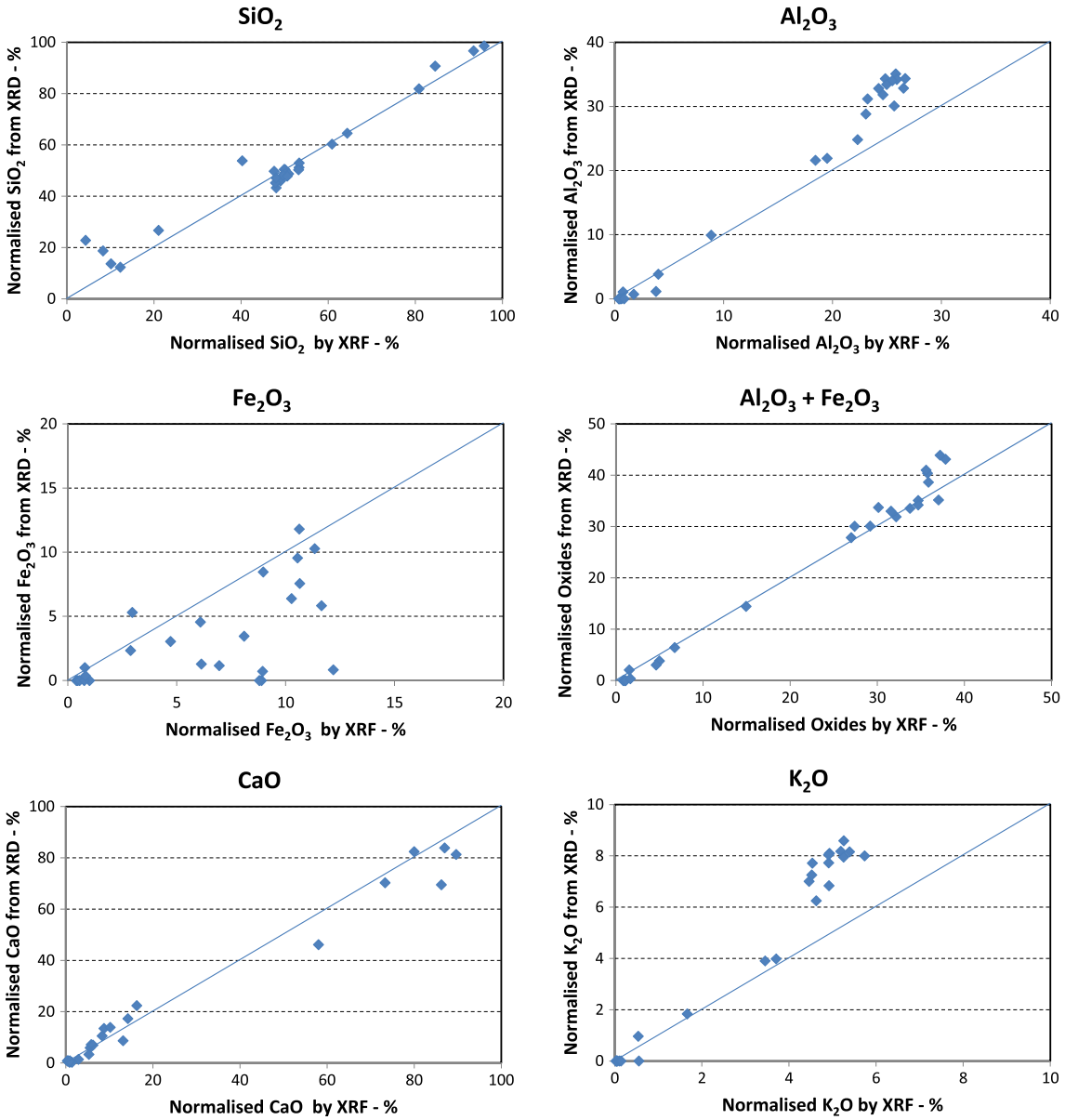

Fig. 10 Relationship of major element oxide percentages (normalized, SO_3-free) inferred from XRD data to percentages of the same oxide (normalized, SO_3-free) obtained by XRF analysis

between the sum of Al_2O_3 and Fe_2O_3 in the samples (Fig. 10) shows quite good agreement between the observed and inferred percentages, suggesting that the low inferred values for Fe_2O_3 are balanced by high inferred values in the same samples for Al_2O_3, and hence that some of the Al has been replaced by Fe in the illite and/or I/S components.

The plot for K_2O shows good agreement between observed and inferred percentages for the samples with K_2O percentages less than 4 % (left-hand side of the plot). These represent the un-ashed non-coal samples, in which illite and I/S could be recognized as separate phases from the XRD patterns. However, most of the data points for the LTA samples from the coal, which correspond the points with higher K_2O percentages (>4 %), plot somewhat above that line. The illite composition used in calculation of the inferred chemistry was based on an illite with K^+ ions in the interlayer positions, and hence this observation suggests that ions other than K^+ are also present in the illite for those particular coal samples.

However, as indicated above, the material identified as illite in the LTAs, especially those of the coals from the HST and LHD mines, may in fact represent a combination of illite and I/S, with the I/S having collapsed to produce a more simple illite structure due to heating in the low-temperature ashing process. A deficiency of K^+ ions would be expected in the mixed-layer I/S, relative to that of a stoichiometric illite, and the fact that I/S was present but not allowed for in the calculations could explain the difference between the inferred and observed percentages of K_2O for these materials.

Figure 11 shows a plot of the combined percentage of pyrite and marcasite, expressed as a fraction of the original coal sample, against the percentage of pyritic sulphur for the same samples as determined by conventional analysis methods. A line showing the expected relationship between these two parameters, based on mineral stoichiometry, is also shown on the figure. The plot shows a relatively good correlation between the percentages of pyrite and pyritic sulfur in the coals but suggests that the percentage of sulfide minerals may have been slightly overestimated by the XRD technique. As indicated by Ward et al. (2001), however, determination of pyrite and other Fe-rich phases by Rietveld-based XRD methods, where the analysis is based on Cu-$K\alpha$ radiation, may be influenced by mass absorption effects. Compensation was made for such effects as part of the Siroquant processing, but variation in the Brindley particle size parameter for the materials studied may have affected the XRD results.

Modes of occurrence of minerals in the Guiding coals

1. Quartz

   Quartz occurs as individual particles in the collodetrinite, with a size generally less than 20 μm (Fig. 12a–c). The modes of occurrence of quartz indicate that it is either of authigenic or detrital origin. Authigenic quartz has commonly been observed in the Late Permian coals from eastern Yunnan and western Guizhou (Ren 1996; Wang et al. 2012). It was previously thought that the quartz was deposited from silica-containing solutions that originated from weathering of basaltic rocks in the Kangdian Upland (e.g., Ren 1996). A small proportion of the quartz also occurs as fracture-fillings (Fig. 12d), indicating an epigenetic origin.
2. Clay minerals

   Three modes of occurrence of clay minerals can be identified (Fig. 13a–d): a large proportion of the mixed-layer I/S is distributed along the bedding planes (Fig. 13a, d); kaolinite, illite, and I/S also occur as cell-fillings (Fig. 13b), or as lath- and needle-shaped forms in the collodetrinite (Fig. 13a, c). The bedding-plane and cell-filling modes of occurrence of the clay minerals indicate a terrigenous and an authigenic origin, respectively, but the lath- and needle-shaped forms suggest detrital material of terrigenous origin. Fine-grained lath- or needle-like particles of illite have been observed in the coal benches and partings of the Heshan Coalfield, and are also thought to represent detrital minerals of terrigenous origin (Dai et al. 2013a). No fracture-filling epigenetic clay minerals were observed in the Guiding coals.
3. Carbonate minerals

   Two modes of occurrence of calcite were observed in the Guiding coals. (1) Intraclasts in collodetrinite. Mixed-layer illite/smectite derived from the sediment-source region is distributed along the edges of the calcite particles (Fig. 13d), suggesting a syngenetic (pre-compaction of peat) origin and formation as an intraclast from the sediment that formed the associated limestones. Shao et al. (1998) also identified terrigenous dolomite in the Heshan coals. (2) As fracture-fillings. Dolomite and calcite fill in fractures within the macerals, indicating an epigenetic origin (Fig. 13e).
4. Sulfide and sulfate minerals

   Sulfide minerals in the Guiding coal include marcasite, pyrite, and a very small proportion of sphalerite. Marcasite occurs as radial aggregates and, in some cases, shows a superimposed layer structure (Fig. 13f). Pyrite occurs as fine-grained crystals in collodetrinite (Figs. 12b, 14a). Some pyrites are corroded and replaced by sulfate minerals (Fig. 14a–d). Sphalerite, with a trace amount of Cd, was also identified in the coal by SEM-EDS techniques.

   Sulfate minerals detected in the Guiding coal samples by XRD and SEM-EDX include jarosite, crystalline $FeSO_4(OH)$ (Fig. 14a, b), and water-bearing Fe(Si)-oxysulfate (Fig. 14b–d). The $FeSO_4(OH)$ is generally distributed along the edge of corroded pyrite crystals (Fig. 14a, b) and was probably derived from pyrite oxidation. Water-bearing Fe-oxysulfate is distributed both in collodetrinite and in the cavities of corroded pyrite (Fig. 14c, d). The modes of occurrence of the water-bearing Fe(Si)-oxysulfate suggest its derivation from reactions between pyrite oxidation products and Si-bearing solutions.

   Jarosite ($KFe^{3+}{}_3(OH)_6(SO_4)_2$) was identified by XRD studies in some of the coal samples (Fig. 14e). This mineral may have been derived from the oxidation of iron sulfides, as found in previous studies (cf. Rao and Gluskoter 1973). It occurs as lath-like or as irregular-shaped masses in collodetrinite, or is more evenly

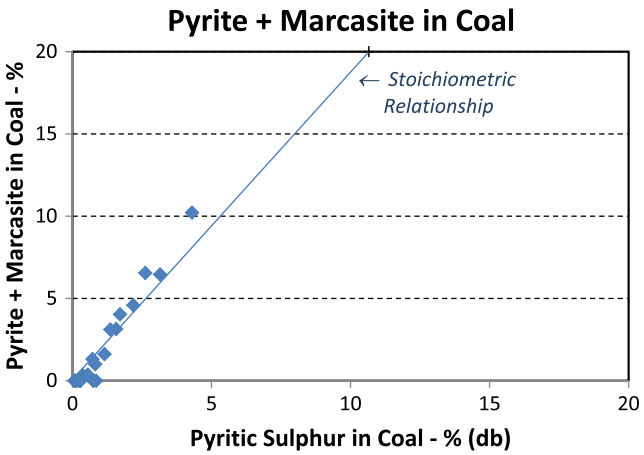

Fig. 11 Plot showing relationship of pyrite plus marcasite as a fraction of the host coal compared to the percentage of pyritic sulfur in the same coal samples

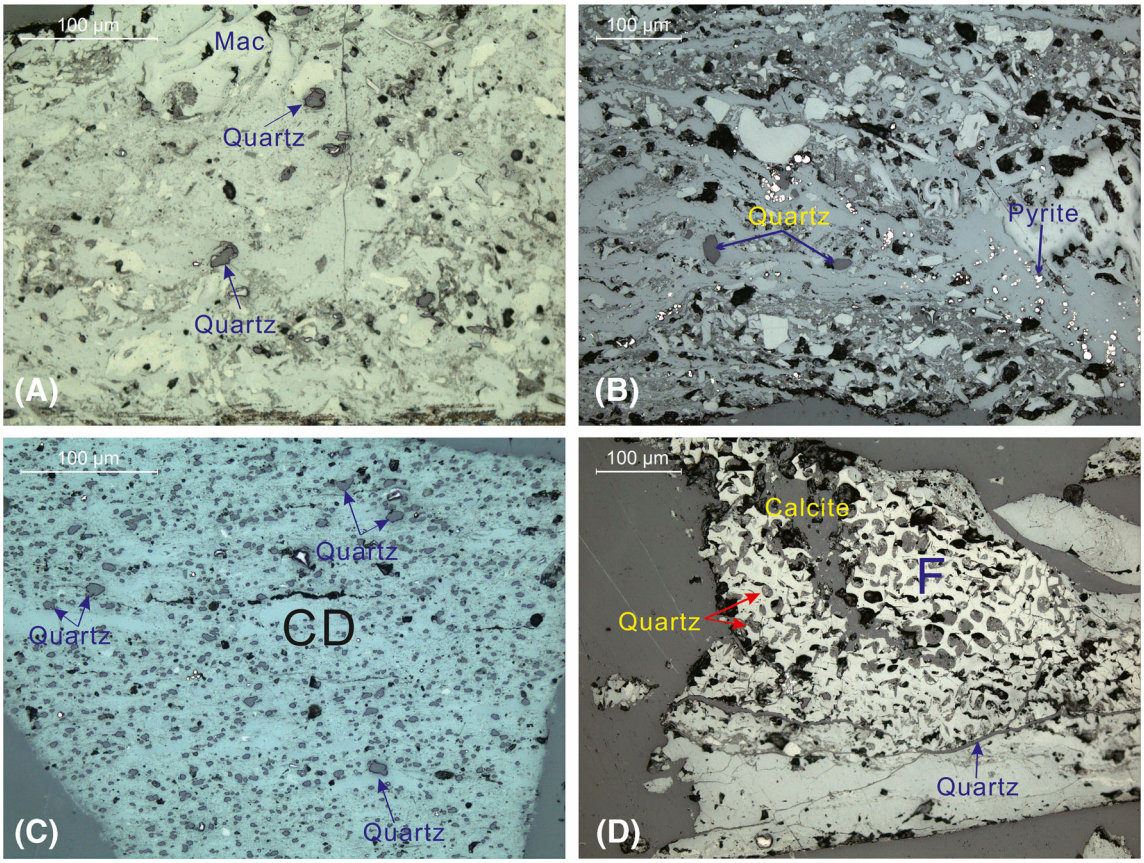

Fig. 12 Optical photomicrographs of quartz and pyrite in the Guiding coals, reflected light. **a** Quartz in sample GC-3C; **b** quartz and pyrite in sample HST-3-1; **c** quartz in sample LHD-1C; **d** quartz filling in fractures of sample GC-3C. *Mac*, macrinite; *CD*, collodetrinite; *F*, fusinite

distributed within the collodetrinite (Fig. 14e, f).

Gypsum occurs as a fracture filling in the samples (Fig. 15), and was possibly produced by reactions between calcite and the sulfuric acid produced by oxidation of pyrite in the coal (cf. Rao and Gluskoter 1973; Pearson and Kwong 1979; Ward 2002). In some low-rank coals, however, gypsum is thought to have formed by evaporation of pore water in fractures and on exposed coal surfaces (Kemezys and Taylor 1964; Ward 2002).

5. Uranium-bearing minerals

Small proportions of some U-bearing minerals, coffinite ($U(SiO_4)_{1-x}(OH)_{4x}$) and brannerite (UTi_2O_6), were identified by SEM studies in the Guiding coals (Fig. 16). They are mainly distributed in the organic matter or in the clay minerals (Fig. 16) and probably have an epigenetic origin. It is suggested that U-bearing solutions leached from the coal by hydrothermal activity reacted with Si-bearing hydrothermal solutions, or with Ti-bearing solutions derived from the breakdown of labile Ti-bearing minerals in the coal, to form these U-bearing minerals. Coffinite has been reported in some coals (Van Der Flier and Fyfe 1985; Seredin and Finkelman 2008); however, brannerite has never been reported in coal. The U in the Heshan, Yanshan, and Fusui coals mainly show an organic association, and no U-bearing minerals have been identified in those deposits (Dai et al. 2008, 2013a, b).

Discussion

Previous studies suggest that SHOS coals preserved within marine carbonate successions were significantly influenced by seawater (Lei et al. 1994; Shao et al. 2003; Zeng et al. 2005), and thus marine conditions may have had a significant influence on the geochemical anomalies found in such coals (Chou 2012). Recent geochemical and mineralogical studies by Dai et al. (2008, 2013a) have shown that, in addition to seawater, a large proportion of the organic sulfur, as well as much of the U, Se, Mo, V, and Re in the Yanshan and Heshan coals, may have been derived from hydrothermal fluids, possibly including fluids of submarine exhalative origin.

Origin of high sulfur content

The syngenetic incorporation of sulfur into coal is linked to the paleosalinity of the original peat-forming environment. In

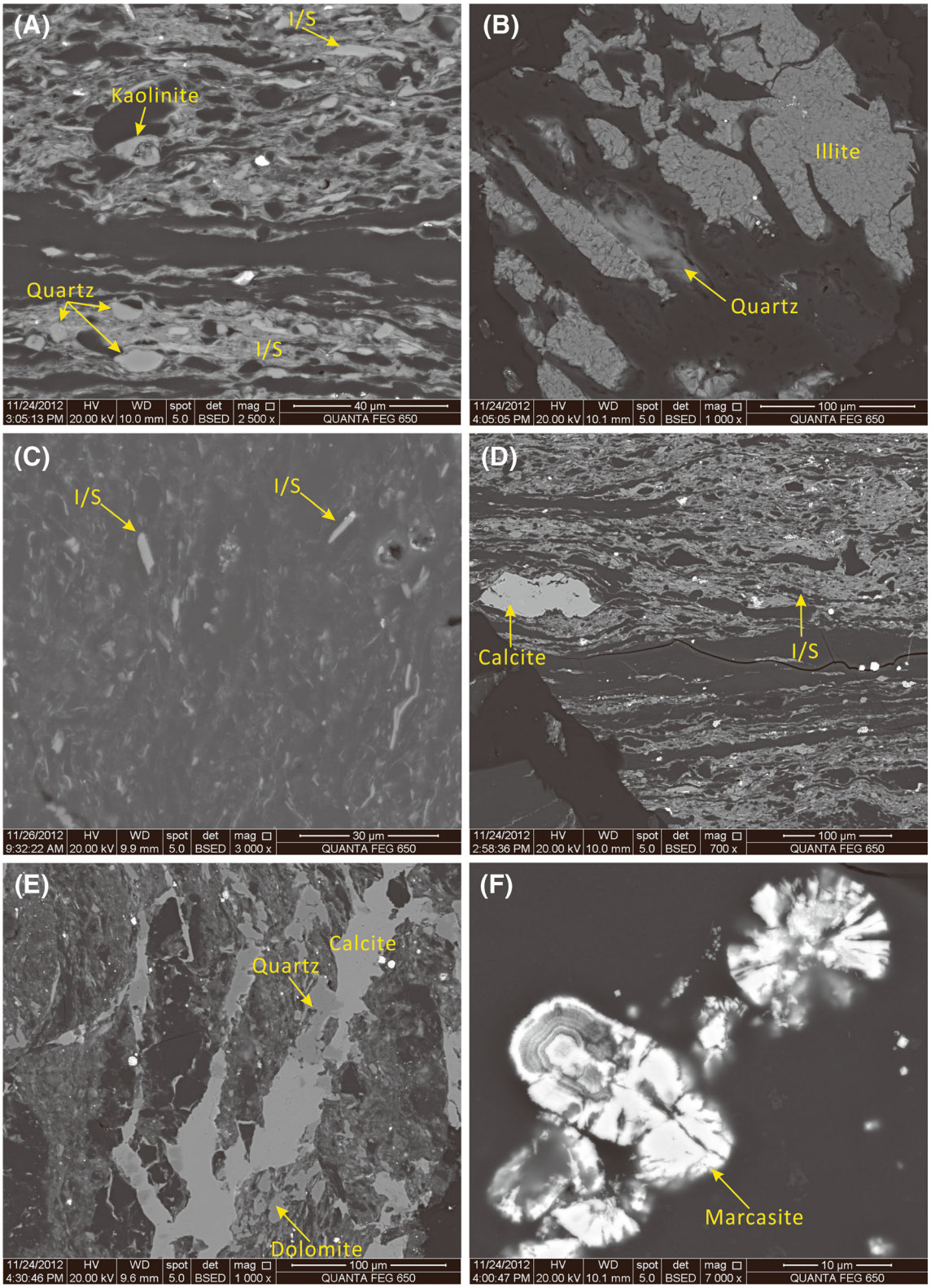

Fig. 13 SEM back-scattered images of clay, carbonate, sulfide, and quartz in the Guiding coal. **a** Kaolinite, mixed-layer illite/smectite (I/S), and quartz in sample GC-1C; **b** cell-filling illite and fracture-filling quartz in sample GC-1C; **c** mixed-layer I/S in collodetrinite in sample GC-1C; **d** mixed-layer I/S occurring in plane beddings and along with the edge of calcite in sample GC-1C; **e** fracture-filling calcite, dolomite, and quartz in sample GC-8-1; **f** marcasite in sample GC-1C. *CD* collodetrinite

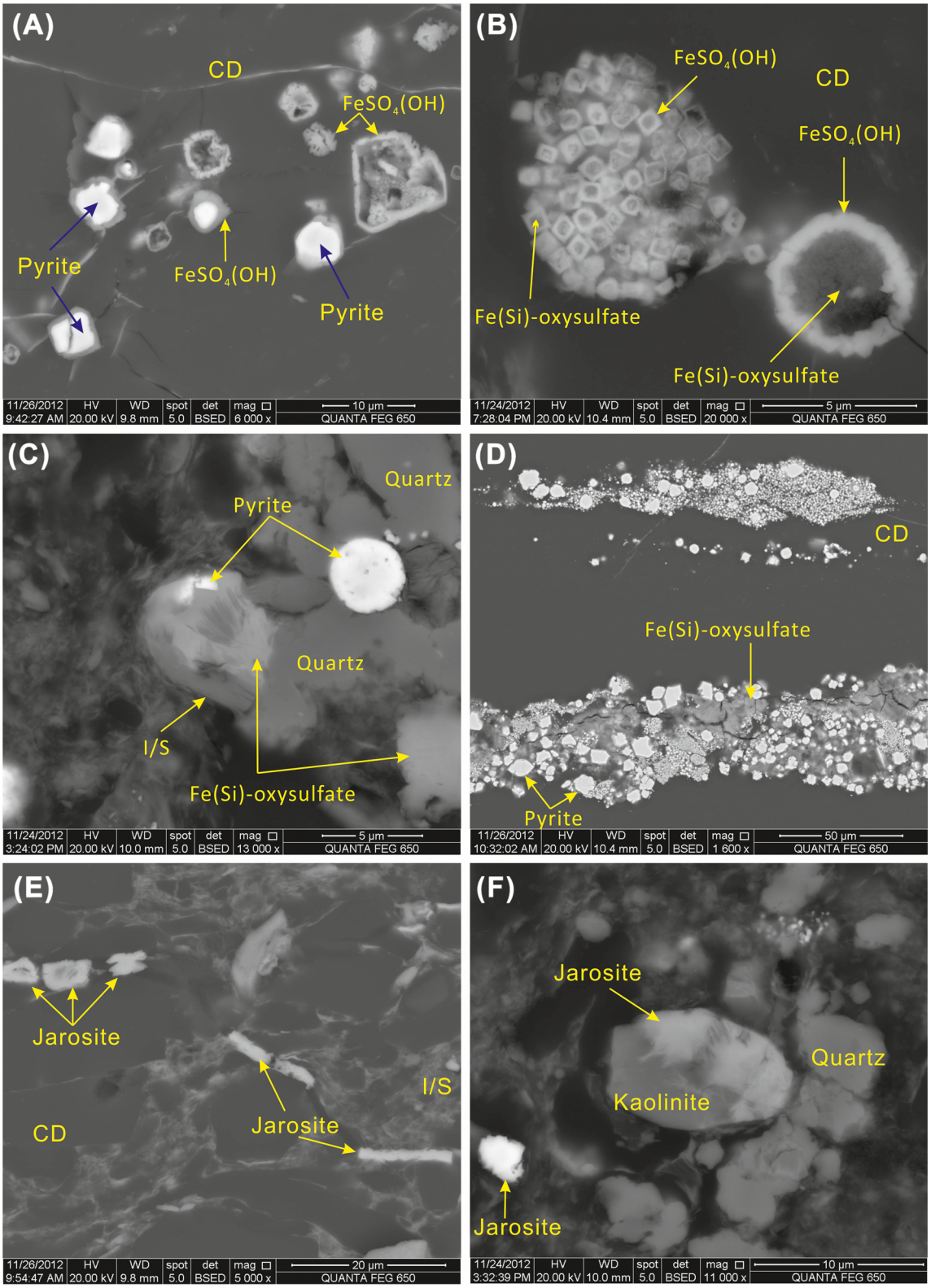

Fig. 14 SEM back-scattered images of Fe-bearing sulfate or oxysulfate in the coal. **a** $FeSO_4(OH)$ and corroded pyrite in sample GC-3-1; **b** $FeSO_4(OH)$ and Fe(Si)-oxysulfate in sample GC-3-2; **c** Fe(Si)-oxysulfate, pyrite, quartz, and mixed-layer I/S in sample GC-1C; **d** Fe(Si)-oxysulfate and pyrite in sample HST-3C; **e** jarosite in the collodetrinite of sample LHD-1C; **f** jarosite distributed in kaolinite of sample GC-2-C

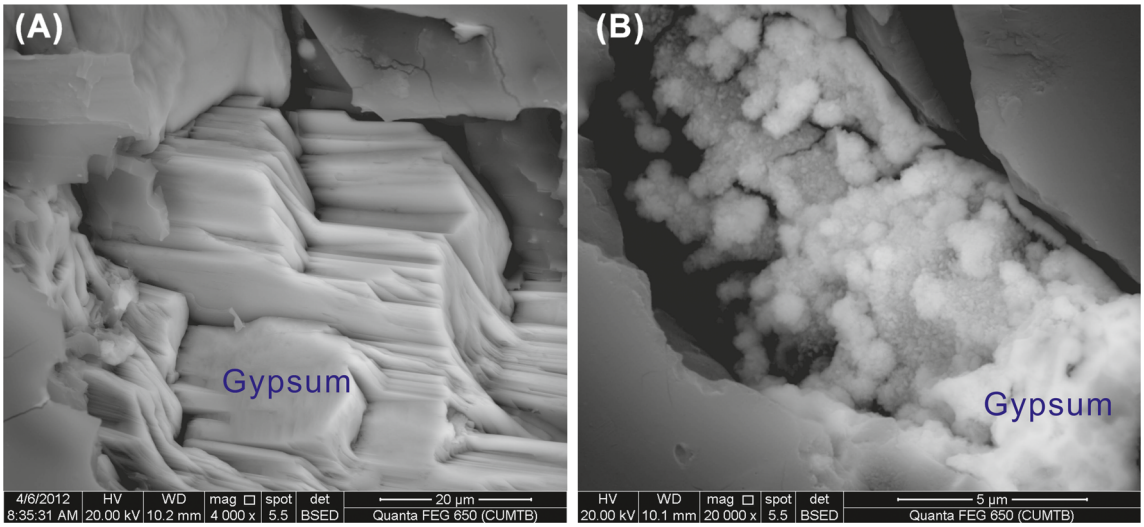

Fig. 15 SEM back-scattered images of gypsum filled fractures in sample GC-3-2

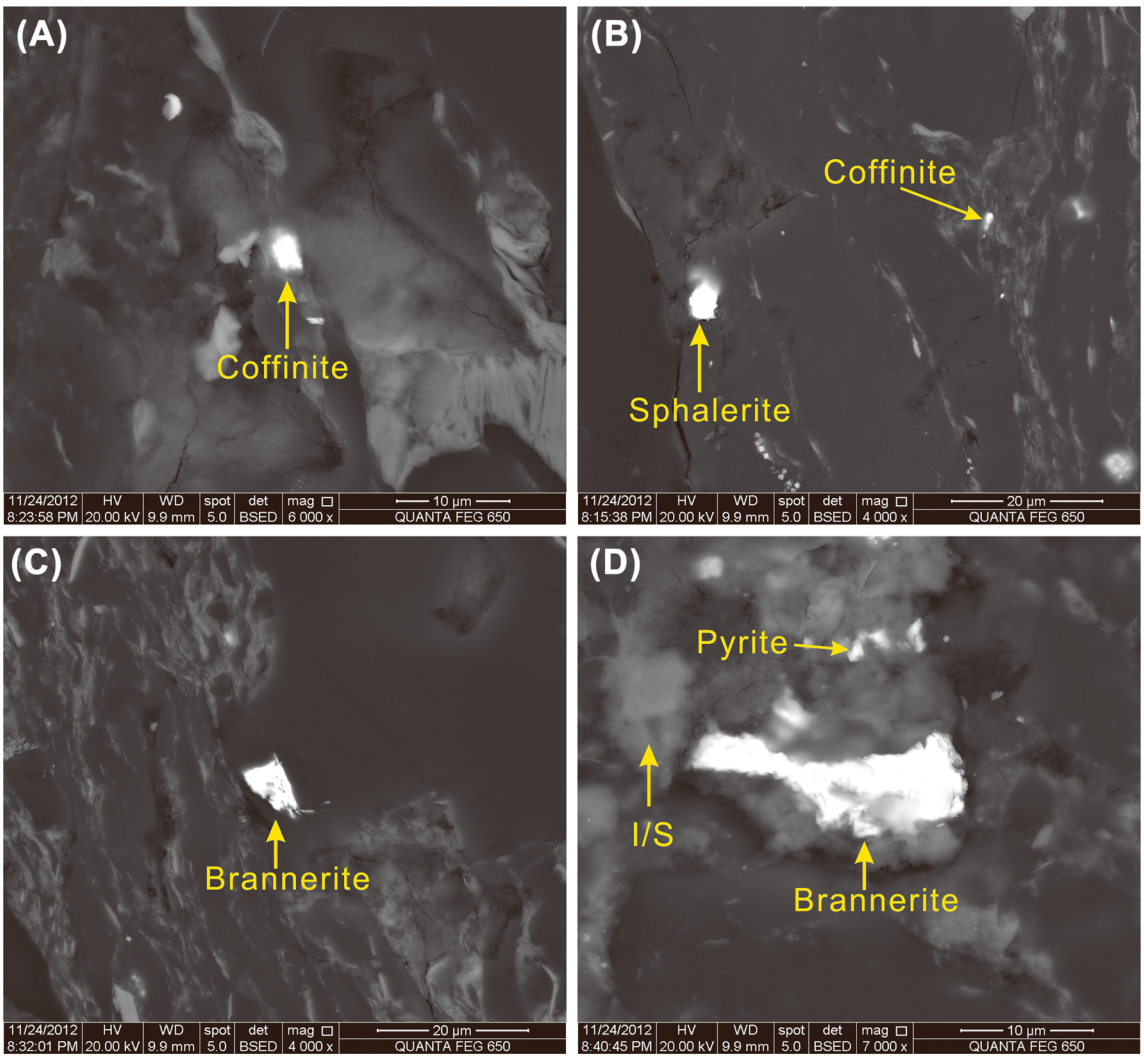

Fig. 16 SEM back-scattered images of U-bearing minerals in sample GC-3-2. **a** Coffinite in organic matter; **b** coffinite in clay minerals and sphalerite in organic matter; **c** brannerite in organic matter; **d** brannerite and pyrite in mixed-layer I/S

most cases, low-sulfur coals were formed in fluvial environments and high-sulfur coals were deposited in seawater-influenced environments, reflecting a greater availability of seawater sulfate under marine conditions (Chou 1997a, b, 2012; Ward et al. 2007). For example, based on observations in the Herrin coal bed in the Illinois Basin, Chou (1990) concluded that the elevated concentrations of sulfur, as well as B, Mo, and U, were probably derived from seawater that flooded the swamp and terminated peat accumulation (Chou 1984, 1997a, b).

Super-high organic sulfur coals are generally considered to have been formed in a clastic-starved basin with accumulation of algae and significant seawater influence (Chou 2012). A number of studies have also indicated that the Late Permian coals preserved within marine carbonate successions at Heshan and Guiding were deposited in restricted marine-influenced environments (Shao et al. 1998, 2003; Zeng et al. 2005).

However, there are also examples of high-sulfur coals that were not subjected to seawater influence. For example, the high-sulfur Miocene lignites (up to 8.2 % total sulfur) in the Çayirhan coalfield, Beypazari Basin, Central Anatolia, Turkey, were deposited in a non-marine environment; sources of sulfur in those coals have been attributed to volcanoclastic or clastic materials and basinal fluids (Whateley and Tuncali 1995a, b). Sulfur enrichment (0.4–12.2 %) in the Miocene lignite of the Çan Basin, northwestern Turkey, was attributed to regional volcanic activity and sulfide mineralization (Gürdal 2011; Gürdal and Bozcu 2011). These high-sulfur Turkish lignites formed in freshwater environments, with the sulfur derived from sources other than seawater.

It is possible that a proportion of the organic sulfur in the Guiding coals in this study was derived from seawater. The Guiding coals were formed on a restricted carbonate platform, as described above; if fresh seawater was not replenished, it could result in a limited system for sulfur formation. Moreover, the concentration of SO_4^{2-} in paleo-seawater is within a certain range. For example, the SO_4^{2-} content of Phanerozoic seawater was in the range of 5 to 27.6 mmol/kg (Lowenstein et al. 2003; Strauss 2004). Seawater might have significantly contributed to the sulfur content of the coal. The $\delta^{34}S$ values for organic and pyritic sulfur are from −7.4 to +7.7‰ and from −28.2 to −30.6‰, respectively (Lei et al. 1994), indicating a euxinic environment and bacterial reduction under sulfate limitation, i.e., a partly closed basin with cyclic supply of seawater sulfate (Turner and Richardson 2004; Elswick et al. 2007; Jiang et al. 2008; Chou 2012).

The $\delta^{34}S$ values of organic sulfur in other high-sulfur coals, where total sulfur content is greater than 1 %, are also variable and typically have more depleted values. For example, these values were found to range −8 to +15‰ in the coals from Illinois Basin, USA (Price and Shieh 1979); the SHOS coals of Tertiary age along the on-shore margin of the Gippsland Basin (Victoria, Australia) have an organic sulfur content between 5.2 and 7.4 %, $\delta^{34}S$ values of organic sulfur between +2.9 and +24.4‰ (Smith and Batts 1974); and $\delta^{34}S$ values are from −12.3 to +5.8‰ in coals from Inner Mongolia, China (Dai et al. 2002). These $\delta^{34}S$ values of organic sulfur also suggest a significant contribution from bacteriogenic processes during biochemical alteration of plant debris.

Boron in the coal

Boron concentration in coal can be used as a paleosalinity indicator for the original sedimentary environment (Goodarzi and Swaine 1994; Eskenazy et al. 1994; Cairncross et al. 1990). For example, Goodarzi and Swaine (1994) placed the fresh/brackish and brackish/marine boundaries at 50 and 110 μg/g B as indices of coal-forming sedimentary environments. Those values have been widely used by others (Alastuey et al. 2001; Hower et al. 2002; Kalkreuth et al. 2010). However, the use of B as a paleosalinity indicator remains controversial (Eskenazy et al. 1994; Lyons et al. 1989). For example, an elevated concentration of B in coal may also be derived from hydrothermal activity (Lyons et al. 1989), volcanic activity (Bouska and Pesek 1983, Karayigit et al. 2000), and climatic variations (Bouska and Pesek 1983).

On the other hand, although the B concentration is more than 400 times higher in seawater than in river water (Li 1982), some studies have shown that coals preserved within carbonate successions or coals significantly influenced by seawater are not necessarily enriched in B. For example, some Late Permian coals from Fusui (Dai et al. 2013b) and Heshan (Dai et al. 2013a), as well as the Guiding coals in this study (Table 2), have a low B concentrations. The nos. 9 and 10 coals from the Wuda Coalfield (Inner Mongolia, China), which were subjected to significant marine influence (Peng and Zhang 1995; Dai et al. 2002), have extraordinarily low B concentrations, from below the ICP-MS detection limit to 10.4 μg/g, with an average of 4.26 μg/g. Dai et al. (2013b) attributed the low B in coals preserved within such carbonate successions to the impermeable interlayered mudstone or siliceous rocks between the coal and limestone roof strata, which prevented the infiltration of the seawater into the coal seam. However, the reasons for the low B concentration in the coals with immediate roof strata of limestone as seen in this study, or in coals without limestone roof strata but significantly influenced by seawater (e.g., Wuda coals in Inner Mongolia; Dai et al. 2002; Peng and Zhang 1995), still remain unclear.

Moreover, it is not sure whether the high B concentration in the coals preserved within such carbonate successions (e.g., 323 μg/g B in the Yanshan coals, Ren et al. 2006; 135 μg/g B in the Heshan coals, Dai et al. 2013a) was derived from seawater because those coals were also significantly influenced by hydrothermal fluids (Dai et al. 2008, 2013a), which

could have provided a source for the B in the coal (Lyons et al. 1989).

Indications of other elements in coal

In addition to B, elements such as Cl, Li, Mg, Ca, Na, F, Sr, and Rb, which are two to four orders-of-magnitude more abundant in seawater than in freshwater (Cairncross et al. 1990; Reimann and de Caritat 1998), would be expected to be enriched in coals influenced by seawater. Numerous studies showed that peats and coals formed in a marine-influenced environment are enriched in these elements (e.g., Raymond Jr et al. 1990; Eskenazy et al. 1994, 2013; Hickmott and Baldridge 1995; Chou 1997a, b; Liu et al. 2004, 2006; Tang and Huang 2004; Song et al. 2007; Yossifova 2014), not only because seawater contains higher contents of these elements than freshwater but also because plankton in marine water are enriched in these elements and can also change the pH, Eh, and H_2S content, leading to a favorable environment for enrichment of trace elements (Ren et al. 2006; Wang et al. 2007; Tang and Huang 2004). Note that the role of the element solubility in the enrichment of elements in coals influenced by a marine environment needs further investigation. However, some SHOS coals are not rich in these elements (Figs. 3, 4). For example, the concentrations of Li, Rb, Sr, and Cl in the Yanshan coals; Rb and Sr in the Chenxi coals; and Cl, Rb, and Sr in the Fusui coals, are close to or even lower than their averages in world hard coals (Ketris and Yudovich 2009).

Relatively low concentrations of elements (e.g., Li, B, F, Cl, Sr, and Rb) expected to be enriched in some SHOS coals (e.g., Yanshan, Chengxi, Fusui) suggest that the high organic sulfur in the coal is due to hydrothermal fluids (Dai et al. 2008, 2013b). However, the absence or very weak influence of seawater on the chemical composition of some Fusui SHOS coals may be due to the screening by an impermeable clay or siliceous layer immediately overlying the coal seam, insulating it from seawater effects during accumulation of the overlying limestone strata.

Significant seawater influence on some Heshan SHOS coals is supported by the high concentration of some elements (e.g., B, Mg, K, Sr, Rb) (Dai et al. 2013a). The higher ratio of Sr/Ba through the seam section than the average for world coals (0.67) may, for example, indicate a significant seawater influence. As indicated by Dai et al. (2013a), high concentrations of S, V, Mo, and U that occur through coal seam sections were probably largely derived from hydrothermal solutions during peat accumulation or in the early diagenetic stages, although a proportion of these elements may have derived from seawater.

The HREY enrichment observed in the coal seams (Fig. 5) may be attributed to hydrothermal solutions (Michard and Albarède 1986; Seredin and Dai 2012). Some studies have shown that natural solutions that may circulate in coal basins (Seredin 2001), including those of alkaline terrestrial waters (Johanneson and Zhou 1997), some high pCO_2 cold mineral waters (Shand et al. 2005), some low-temperature (130 °C) alkaline hydrothermal solutions (Michard and Albarède 1986), and high-temperature (>500 °C) volcanogenic fluids (Rybin et al. 2003), are enriched in HREY. However, the REY in coals dominantly derived from sediment-source region (e.g., granite-, carbonatite-, or bauxite-dominated terrigenous regions) are usually characterized by an L-REY enrichment type (Seredin and Dai 2012; Dai et al. 2014a). For example, the REY in the Late Permian coals from the Xinde mine, Xuanwei, eastern Yunnan Province, were derived from the basaltic Kangdian Upland (Fig. 1a) and are characterized by L- and M-REY enrichments (Dai et al. 2014a). In addition, the REY in the Heshan and Yanshan coals that were derived from the northern Vietnam Upland and Yunkai Upland (both mainly composed of felsic rocks; Li and Xu 2000; Chen et al. 2003; Feng et al. 1994) would be expected to have a L-REY enrichment type, but are characterized by H-REY enrichment, due to the influence of hydrothermal fluids (Dai et al. 2008, 2013a).

Although the H-type REY distribution pattern as an indicator of hydrothermal solution injection, the high U/Th ratio in the Guiding coals in this study (75.0 for GC-3 seam, 68.5 for HST-3 seam, and 120 for LHD-1C), as well as in coals from Heshan (3.9 on average, Dai et al. 2013a), Yanshan (16.9 on average; Dai et al. 2008), and Chenxi (16.9 on average; Li and Tang 2013), suggest an euxinic environment (Bostrom et al. 1973; Bostrom 1983; Dai et al. 2008). However, the U/Th ratio for world hard coals is only 0.6 on average (Ketris and Yudovich 2009). The concentration of authigenic uranium can be also considered as an indicator of sedimentary environment (Wignall 1994). The concentration of authigenic uranium (U_a) is calculated as $U_a = U_{Total} - Th/3$. The U_a values for samples LHD-1C (228 μg/g), GC-1C (286 μg/g), GC-3 (198 μg/g), and HST-3 (201 μg/g) indicate that the Guiding coals were deposited in a euxinic environment in which uranium was remarkably enriched. Similarly, the concentrations of authigenic uranium in the Heshan (42.3 μg/g on average; Dai et al. 2013a), Yanshan (150 μg/g on average; Dai et al. 2008), and Chenxi (73.7 μg/g on average; Li and Tang 2013) coals are also high. The average U_a for the world hard coals is only 0.83 μg/g (Ketris and Yudovich 2009).

General characteristics of U-bearing SHOS coals

The enrichment of trace elements in coal is usually attributed to a combination of geological processes during peat accumulation and subsequent diagenetic and epigenetic activities.

Seredin and Finkelman (2008) described two types of U enrichment in coal, as well as the accompanying enrichment of Se, Mo, Re, and V:

1. *Epigenetic infiltration type*. The enrichment of these trace elements is attributed to epigenetic infiltration solution circulation in the coal basin at the lignite to subbituminous stage, which usually leads to large U deposit formation. In addition to Mo, Se, V, and Re, which normally accompany the U and are enriched in the U-bearing coals, other lithophile, chalcophile, and siderophile elements (e.g., Co, Cu, Zn, Ge, Se, Y, Ag, Th, Be, REE, Zr, and Tl) are generally enriched as well. The coal basins are surrounded by rocks significantly enriched in U, and the climate was arid during the epigenetic infiltration process. The optimal hydrologic condition for enrichment of coal by these elements involves a high proportion of coarse sediments serving as channels for migration of the U-bearing solutions.
2. *Syngenetic or early diagenetic infiltration and exfiltration types*. This kind of U-bearing coal deposit is usually much smaller than the typical epigenetic infiltration type. The coal beds usually are interlayered between impermeable clays, which prevent injection of the epigenetic solutions into the coal seam. The coal deposits are located in the marginal parts of coal basins. The enrichment of U in the syngenetic or early diagenetic exfiltration type is characterized by structural control for the coal deposits, metasomatic alteration in the basement rocks, high (up to 3–6 m) thickness of the U-rich layers, small areas for the deposits, and location of U mineralization in several beds lying at different vertical levels and in adjacent non-coal rocks. Coals of this deposit type usually contain W, which is normally absent from the infiltration type of uranium deposits.

The U-bearing coals from the Guiding, Heshan, Chenxi, and Yanshan coalfields that are preserved within carbonate successions are also enriched in Se, Mo, Re, and V. However, the origin of these elevated trace-element concentrations and the general characteristics of these coal deposits are different from those of the two types of U-bearing coal deposits described by Seredin and Finkelman (2008). The coals from the Guiding, Heshan, Chenxi, and Yanshan coalfields have the following characteristics:

1. All the SHOS coals of southern China with elevated concentrations of U, Se, Mo, Re, and V are of Late Permian age. However, the other U-bearing coal deposits of epigenetic infiltration type are of Paleozoic, Mesozoic, and Cenozoic age (Seredin and Finkelman 2008).
2. The elements S, U, Se, Mo, Re, and V were largely derived from exfiltrational hydrothermal solutions during peat accumulation (e.g., Yanshan and Heshan coals as reported by Dai et al. 2008, 2013a, respectively) or were deposited in an euxinic environment (e.g., Guiding coals in the present study).
3. All the SHOS coals are intercalated with marine carbonate rocks. In most cases, the roof strata are limestones (or siliceous and bioclast-rich limestones), and, in some instances, a thin impermeable mudstone or siliceous layer is located between the coal and the roof limestone. The floor strata of the SHOS coals are limestones or mudstones.
4. The thickness of the SHOS coal beds is generally less than 2 m. The thickness of the U-bearing portion of the other coal beds, as described by Seredin and Finkelman (2008), is 0.1–0.5 m in most cases and rarely exceeds 1–2 m.
5. The sediment-source regions for the SHOS coals of individual coalfields are different. For example, the northern Vietnam Upland was the terrigenous sediment source for the Yanshan coals (Dai et al. 2008), the Yunkai Upland for the Heshan and Fusui coals (Dai et al. 2013a, b), and the Jiangnan Upland for the Chenxi coals (Li and Tang 2014) (Fig. 1a). These sediment-source regions have different lithological compositions, e.g., the northern Vietnam Upland is mainly composed of rhyolite (Li and Xu 2000; Chen et al. 2003) and the Yunkai Upland is dominated by felsic Permo-Carboniferous rocks (Feng et al. 1994). The basaltic Kangdian Upland (Fig. 1a) provided the sediment source region for the Late Permian Guiding coals (China National Administration of Coal Geology 1996).
6. The trace elements with elevated concentrations (U, Mo, and V) have a mixed mode of occurrence, but mainly occur in the organic matter. The concentration of U in the SHOS coal beds varies from several tens of microgram per gram to ~200 μg/g. However, the host rocks (roof and floor strata) are not enriched in these trace elements (see Electronic Supplementary File). The U resources of SHOS coals may be less than those of the epigenetic infiltration deposits reported by Seredin and Finkelman (2008).
7. The distributions of U, Se, Mo, Re, and V through the vertical section are more even (as shown in Table 2 and data from Dai et al. 2013a) than in the epigenetic infiltration type of deposit (Seredin and Finkelman 2008). Uranium in the coal beds of the epigenetic infiltration deposits varies significantly through the vertical section, with the highest concentrations occurring in the upper portions at the contacts with oxidized roof strata (Seredin and Finkelman 2008).

Potential economic significance of the rare metals in SHOS coals

As mentioned above, rare metals, including U, Se, Mo, Re, V, and, in some cases, rare earth elements and yttrium, are significantly enriched in the SHOS coals (Table 7), with concentrations up to several hundred times higher than the average values in world coals, and thus the economic significance of their combustion products (e.g., fly and bottom ash) are worthy of further attention. With the exception of V, Se, Mo, and U in the Fusui coals, REY in the Guiding coals, and V in the Heshan coals (Table 7), other rare metals in these SHOS coals, especially REY, Re, and U, may have potential economic significance.

Molybdenum, U, and V are not classified as volatile elements during coal combustion (Clarke and Sloss 1992), and thus would not be expected to be significantly fractionated between fly and bottom ashes. However, some studies have shown that these elements are significantly enriched in fly ash compared to bottom ash (e.g., for V partitioning: Dai et al. 2014b; for Mo partitioning: Qi et al. 2011), which may be due to their organic mode of occurrence in the feed coal (Dai et al. 2014b). Owing to the high volatility of Se and its capture from the gas phase on ash particles, the Se concentration in fly ash may be 20 to 100 times higher than that in the raw feed coals (Seredin et al. 2013; Swanson et al. 2013). However, REY do not show significant fractionation between fly and bottom ashes, although REY tend to be enriched in the finer fly ashes among the size-fractioned fly ashes (Hower et al. 2013), and thus both fly ash and bottom ash should be considered as potential REY sources.

Table 7 Concentration of rare metals, Cr, Ni, and Cd in coal ash (μg/g unless indicated as %)

Sample No.	V	Se	Mo	Re	REO	U	Sum-RM (%)	Cr	Ni	Cd
GC-1C	4,948	127	2,026	3.26	181	1,236	0.83	1,979	575	28.7
GC-3-1	2,880	160	436	4.85	197	326	0.38	2,270	486	9.19
GC-3-2	5,367	142	1,724	4.67	235	1,300	0.85	3,223	833	19.8
GC-3-3	6,212	180	2,563	0.33	411	1,166	1.01	2,384	345	14.9
GC-3-4	4,939	182	2,442	0.55	441	1,184	0.87	2,245	353	15.3
GC-3-5	3,446	197	2,302	0.43	453	1,058	0.70	1,468	253	11.2
GC-3B-Av	4,559	174	1,984	2.03	358	1,057	0.78	2,284	451	14.3
GC-3C	4,256	179	1,466	2.27	305	887	0.68	2,303	462	13.8
HST-3-0	1,778	231	536	0.28	241	220	0.28	1,346	284	10.1
HST-3-1	6,806	121	1,599	1.24	272	1,161	0.97	2,012	628	16.2
HST-3-2	6,352	98	3,028	0.49	477	1,894	1.14	1,669	663	20.1
HST-3-3	2,143	150	1,066	0.30	394	658	0.40	807	316	12.5
HST-3-4	727	114	347	0.12	365	135	0.13	490	142	5.90
HST-3B-Av	2,732	151	1,092	0.35	347	638	0.46	1,113	341	11.5
HST-3C	3,566	138	1,570	0.55	404	949	0.62	1,140	413	14.0
LHD-1C	4,941	84	2,479	0.83	336	1,355	0.89	1,456	525	18.3
GC-3	4,408	176	1,725	2.15	332	972	0.73	2,293	456	14.1
HST-3	3,055	146	1,277	0.43	369	758	0.52	1,124	369	12.5
All Guiding coals	3,998	152	1,652	1.49	337	950	0.68	1,754	440	15.1
Yanshan coal[a]	2,061	91.6	742	1.1	941	556	0.44	1,196	269	7.50
Fusui coal[b]	147	22.9	27.3	nd	1170	21.0	0.12	107	35.6	2.77
Heshan coal[c]	381	35.5	125	nd	767	126	0.14	205	48.0	2.20
Chenxi coal[d]	2,120	na	166	nd	1349	539	0.42	2,923	244	35.9
World coal ash[e]	170	10.0	14	nd	534	15	0.074	120	100	1.20

nd no data, *C* channel sample, *Av* weighted average (weighted by thickness of sample interval), *REO* sum of oxides of rare earth elements and yttrium, *Sum-RM* sum of V, Se, Mo, Re, REO, and U, *GC-3* average of M3 seam in Guanchong Mine, *HST-3* average of M3 seam in Heishentian Mine, *3B-Av* weighted average for coal benches of M3 seam (weighted by thickness of sample interval)

[a] From Dai et al. (2008)

[b] From Dai et al. (2013b)

[c] From Dai et al. (2013a)

[d] From Li and Tang (2013) and Li et al. (2013)

[e] From Ketris and Yudovich (2009)

Conclusions

In contrast to other super-high-organic sulfur coals in southern China, the basaltic Kangdian Upland provided the sediment source region for the Guiding Late Permian coals. The Northern Vietnam, Yunkai, and Jiangnan Uplands were the dominant epiclastic source regions for the Yanshan, Heshan/Fusui, and Chenxi coals, respectively.

Like other SHOS coals in southern China, the Guiding coals are highly enriched in S, U, Se, Mo, Re, and V. Uranium, Mo, and V in the Guiding coals are mainly associated with the organic matter. In addition, a small proportion of the U and V occur in coffinite/brannerite and jarosite, respectively. The major carriers of Se are pyrite rather than marcasite. Fluorine and Cl mainly occur in tourmaline and as Cl^- ions adsorbed on the coal's organic matter, respectively. Boron occurs in tourmaline and mixed-layer I/S rather than in illite and organic matter. Rhenium probably occurs in the secondary sulfate and carbonate minerals. Although the Guiding coals were subjected to seawater influence, the concentration of B is very low; the B mainly occurs in mixed-layer illite/smectite and tourmaline, and was probably derived from the sediment-source region.

The U-bearing coal deposits preserved within the carbonate platform sequence in southern China, including the Guiding Coalfield, are different to those of previously reported deposits (epigenetic infiltration type, syngenetic or early diagenetic infiltration and exfiltration type). The general characteristics of such U-bearing deposits include the following: formation age limited to the Late Permian, sulfur and rare metals (U, Se, Mo, Re, V, and REY) appearing to be largely derived from exfiltrational hydrothermal solutions (e.g., Yanshan and Heshan coals) or to be associated with an euxinic environment (e.g. Guiding coal in the present study), coal beds intercalated with marine carbonate rocks, and laterally and vertically uniform distributions of rare metals in the coal seams.

Rare metals, including U, Se, Mo, Re, V, and, in some cases, rare earth elements and yttrium, are significantly enriched in the SHOS coals preserved within the carbonate platform successions, and their combustion products (e.g., fly and bottom ash) may have potential economic significance.

Acknowledgments This paper is dedicated to the memory of Dr. Vladimir V. Seredin. The research was supported by the National Key Basic Research Program of China (no. 2014CB238902), the National Natural Science Foundation of China (no. 41272182), and the Program for Changjiang Scholars and Innovative Research Team in University (IRT13099). We would like to thank Editor-in-Chief Dr. Bernd Lehmann and three anonymous reviewers for their careful reviews and useful comments, which greatly improved the manuscript.

References

Alastuey A, Jiménez A, Plana F, Querol X, Suárez-Ruiz I (2001) Geochemistry, mineralogy, and technological properties of the main Stephanian (Carboniferous) coal seams from the Puertollano Basin, Spain. Int J Coal Geol 45:247–265

ASTM Standard D2492-02 (2002, Reapproved 2007). Standard test method for forms of sulfur in coal. ASTM International, West Conshohocken, PA

ASTM Standard D2797/D2797M-11a (2011) Standard practice for preparing coal samples for microscopical analysis by reflected light. ASTM International, West Conshohocken, PA

ASTM Standard D3173–11 (2011) Test method for moisture in the analysis sample of coal and coke. ASTM International, West Conshohocken

ASTM Standard D3174–11 (2011) Annual book of ASTM standards. Test method for ash in the analysis sample of coal and coke. ASTM International, West Conshohocken

ASTM Standard D3175–11 (2011) Test method for volatile matter in the analysis sample of coal and coke. ASTM International, West Conshohocken

ASTM Standard D3177–02 (2002, Reapproved 2007) Test methods for total sulfur in the analysis sample of coal and coke. ASTM International, West Conshohocken

ASTM Standard D388–12 (2012) Standard classification of coals by rank. ASTM International, West Conshohocken

ASTM Standard D5987–96 (2002, Reapproved 2007) Standard test method for total fluorine in coal and coke by pyrohydrolytic extraction and ion selective electrode or ion chromatograph methods. ASTM International, West Conshohocken

Bostrom K (1983) Genesis of ferromanganese deposits—diagnostic criteria for recent and old deposits. In: Rona PA, Bostrom K, Laubier L, Smith KL Jr (eds) Hydrothermal processes at seafloor spreading centers. Plenum Press, New York, pp 473–489

Bostrom K, Kramemer T, Gantner S (1973) Provenance and accumulation rates of opaline silica, Al, Fe, Ti, Mn, Ni and Co in Pacific pelagic sediment. Chem Geol 11:123–148

Bouska V, Pesek J (1983) Boron in the aleuropelites of the Bohemian massif. 5th Meet. Europ. Clay Groups (Prague), pp 147-155

Bouška V, Pešek J, Sýkorová I (2000) Probable modes of occurrence of chemical elements in coal. Acta Montana Serie B, Fuel, Carbon, Mine rProcess Praha 10(117):53–90

Boyd RJ (2002) The partitioning behaviour of boron from tourmaline during ashing of coal. Int J Coal Geol 53:43–54

Cairncross B, Hart RJ, Willis JP (1990) Geochemistry and sedimentology of coal seams from the Permian Witbank Coalfield, South Africa; a means of identification. Int J Coal Geol 16:309–325

Caswell SA (1981) Distribution of water-soluble chlorine in coals using stains and acetate peels. Fuel 60:1164–1166

Caswell SA, Holmes IF, Spears DA (1984) Water-soluble chlorine and associated major cations from the coal and mudrocks of the Cannock and North Staffordshire coalfields. Fuel 63:774–781

Chen J (1987) A further study on the coalification model of the Upper Permian carbonate coal measures in southern China Proc of the Symp on China's Permo-Carboniferous Coal-Bearing Strata and Geology. Science Press, Beijing, pp 217–223 (in Chinese)

Chen C, He B, Gu X, Liu J (2003) Provenance and tectonic settings of the middle Triassic turbidites in Youjiang Basin. Geotecton Metallog 27:77–82

Chen J, Liu G, Jiang M, Chou C-L, Li H, Wu B, Zheng L, Jiang D (2011) Geochemistry of environmentally sensitive trace elements in Permian coals from the Huainan coalfield, Anhui, China. Int J Coal Geol 88:41–54

China National Administration of Coal Geology (1996) Sedimentary environments and coal accumulation of Late Permian Coal Formation in Western Guizhou, Southern Sichuan and Eastern Yunnan China. Chongqing University Press, Chongqing, pp 1–275 (in Chinese with English abstract)

Chou C-L (1984) Relationship between geochemistry of coal and the nature of strata overlying the Herrin Coal in the Illinois Basin, U.S.A. Memoir Geol Soci China 6:269–280

Chou C-L (1990) Geochemistry of sulfur in coal. In: Orr WL, White CM (eds) Geochemistry of sulfur in fossil fuels. American Chemical Society, Washington, DC, pp 30–52

Chou C-L (1997a) Geological factors affecting the abundance, distribution, and speciation of sulfur in coals. In: Yang Q (ed) Geology of fossil fuels—coal. Proc of the 30th Int Geol Congr, Part B, vol. 18. VSP, Utrecht, The Netherlands, pp 47–57

Chou C-L (1997b) Abundances of sulfur, chlorine, and trace elements in Illinois Basin coals, USA. Proc of the 14th Annual Pittsburgh Coal Conference, Taiyuan, Shanxi, China, September 23–27, pp. 76–87

Chou C-L (2004) Origins and evolution of sulfur in coals. West n Pac Earth Sci 4:1–10

Chou C-L (2012) Sulfur in coals: a review of geochemistry and origins. Int J Coal Geol 100:1–13

Clarke LB, Sloss LL (1992) Trace elements-emissions from coal combustion and gasification. IEA Coal Research, London (111pp)

Dai S, Ren D, Tang Y, Shao L, Li S (2002) Distribution, isotopic variation and origin of sulfur in coals in the Wuda coalfield, Inner Mongolia, China. Int J Coal Geol 51:237–250

Dai S, Ren D, Zhou Y, Chou C-L, Wang X, Zhao L, Zhu X (2008) Mineralogy and geochemistry of a superhigh-organic-sulfur coal, Yanshan Coalfield, Yunnan, China: evidence for a volcanic ash component and influence by submarine exhalation. Chem Geol 255:182–194

Dai S, Jiang Y, Ward CR, Gu L, Seredin VV, Liu H, Zhou D, Wang X, Sun Y, Zou J, Ren D (2012a) Mineralogical and geochemical compositions of the coal in the Guanbanwusu Mine, Inner Mongolia, China: further evidence for the existence of an Al (Ga and REE) ore deposit in the Jungar Coalfield. Int J Coal Geol 98:10–40

Dai S, Ren D, Chou C-L, Finkelman RB, Seredin VV, Zhou Y (2012b) Geochemistry of trace elements in Chinese coals: a review of abundances, genetic types, impacts on human health, and industrial utilization. Int J Coal Geol 94:3–21

Dai S, Zhang W, Seredin VV, Ward CR, Hower JC, Wang X, Li X, Song W, Zhao L, Kang H, Zheng L, Zhou D (2013a) Factors controlling geochemical and mineralogical compositions of coals preserved within marine carbonate successions: a case study from the Heshan Coalfield, southern China. Int J Coal Geol 109–110:77–100

Dai S, Zhang W, Ward CR, Seredin VV, Hower JC, Li X, Song W, Kang H, Zheng L, Zhou D (2013b) Mineralogical and geochemical anomalies of late Permian coals from the Fusui Coalfield, Guangxi Province, southern China: influences of terrigenous materials and hydrothermal fluids. Int J Coal Geol 105:60–84

Dai S, Li T, Seredin VV, Ward CR, Hower JC, Zhou Y, Zhang M, Song X, Song W, Zhao C (2014a) Origin of minerals and elements in the Late Permian coals, tonsteins, and host rocks of the Xinde Mine, Xuanwei, eastern Yunnan, China. Int J Coal Geol 121:53–78

Dai S, Seredin VV, Ward CR, Jiang J, Hower JC, Song X, Jiang J, Wang X, Gornostaeva T, Li X, Liu H, Zhao L, Zhao C (2014b) Composition and modes of occurrence of minerals and elements in coal combustion products derived from high-Ge coals. Int J Coal Geol 121:79–97

Damste JAS, White CM, Green JB, de Leeuw JW (1999) Organosulfur compounds in sulfur-rich Raša coal. Energy Fuels 13:728–738

Daybell GN, Pringle WJS (1958) The mode of occurrence of chlorine in coal. Fuel 37:283–292

Elswick ER, Hower JC, Carmo AM, Sun T, Mardon SM (2007) Sulfur and carbon isotope geochemistry of coal and derived coal-combustion by-products: an example from an eastern Kentucky mine and power plant. Appl Geochem 22:2065–2077

Eskenazy G, Delibaltova D, Mincheva E (1994) Geochemistry of boron in Bulgarian coals. Int J Coal Geol 25:93–110

Eskenazy G, Dai S, Li X (2013) Fluorine in Bulgarian coals. Int J Coal Geol 105:16–23

Feng ZZ, Jin ZK, Yang YQ, Pao ZD, Xin WJ (1994) Lithofacies paleogeography of Permian of Yunnan-Guizhou-Guangxi Region. Geological Publishing House, Beijing, 146pp; (in Chinese with English abstract)

Finkelman RB (1980) Modes of occurrence of trace elements in coal. Ph.D. Dissertation. Univ of Maryland, College Park, Md, 301pp

Finkelman RB (1982) The origin, occurrence, and distribution of the inorganic constituents in low-rank coals. In: Shobert HH (ed) Proc Basic Coal Science Workshop (Houston, Texas, 1981) Grand Forts Energy Technol Centre, Grand Forts, ND, pp 69-90

Finkelman RB (1993) Trace and minor elements in coal. In: Engel MH, Macko SA (eds) Organic geochemistry. Plenum, New York, pp 593–607

Finkelman RB (1995) Modes of occurrence of environmentally sensitive trace elements in coal. In: Swaine DJ, Goodarzi F (eds) Environmental aspects of trace elements in coal. Kluwer Academic Publishing, Dordrecht, pp 24–50

Frazer FW, Belcher CB (1973) Quantitative determination of the mineral matter content of coal by a radio-frequency oxidation technique. Fuel 52:41–46

Fu X, Wang J, Tan F, Feng X, Zeng S (2013) Minerals and potentially hazardous trace elements in the Late Triassic coals from the Qiangtang Basin, China. Int J Coal Geol 116–117:93–105

GB/T 15224.1-2004 (National Standard of P.R. China) (2004). Classification for quality of coal. Part 1: Ash yield. (in Chinese)

Gluskoter HJ (1965) Electronic low temperature ashing of bituminous coal. Fuel 44:285–291

Godbeer WC, Swaine DJ (1987) Fluorine in Australian coals. Fuel 66: 794–798

Goodarzi F, Swaine DJ (1994) Paleoenvironmental and environmental implications of the boron content of coals. Geol Surv Can Bull 471: 1–46

Greb SF (2013) Coal more than a resource: critical data for understanding a variety of earth-science concepts. Int J Coal Geol 118:15–32

Gürdal G (2011) Abundances and modes of occurrence of trace elements in the Çan coals (Miocene), Çanakkale-Turkey. Int J Coal Geol 87: 157–173

Gürdal G, Bozcu M (2011) Petrographic characteristics and depositional environment of Miocene Çan coals, Çanakkale-Turkey. Int J Coal Geol 85:143–160

Hickmott DD, Baldridge WS (1995) Application of PIXE microanalysis to macerals and sulfides from the lower Kittanning coal of western Pennsylvania. Econ Geol 90:246–254

Hou X, Ren D, Mao H, Lei J, Jin K, Chu PK, Reich F, Wayne DH (1995) Application of imaging TOF-SIMS to the study of some coal macerals. Int J Coal Geol 27:23–32

Hower JC, Robertson JD (2003) Clausthalite in coal. Int J Coal Geol 53: 221–225

Hower JC, Riley JT, Thomas GA, Griswold TB (1991) Chlorine in Kentucky coals. J Coal Qual 10:152–158

Hower JC, Ruppert LF, Williams DA (2002) Controls on boron and germanium distribution in the low-sulfur Amos coal bed, Western Kentucky coalfield, USA. Int J Coal Geol 53:27–42

Hower JC, Dai S, Seredin VV, Zhao L, Kostova IJ, Silva LFO, Mardon SM, Gurdal G (2013) A note on the occurrence of yttrium and rare earth elements in coal combustion products. Coal Combust Gasification Prod 5:39–47

Huang N, Wen X, Huang F, Wang G, Tao J (1994) The Paleosol bed and the coal deposition model in Heshan coal field, Guangxi, China. Acta Sedimentol Sin 12:40–46 (in Chinese with English abstract)

Huggins FE, Huffman GP (1995) Chlorine in coal: an XAFS spectroscopic investigation. Fuel 74:556–559

Jiang Y, Elswick E, Mastalerz M (2008) Progression in sulfur isotopic compositions from coal to fly ash: examples from single-source combustion in Indiana. Int J Coal Geol 73:273–284

Jin H, Li J (1987) The depositional environment of the Late Permian in the Matan area, Heshan county, Guangxi Province. Sci Geol Sin 20: 61–69 (in Chinese with English abstract)

Johanneson KH, Zhou X (1997) Geochemistry of the rare earth element in natural terrestrial waters: a review of what is currently known. Chin J Geochem 16:20–42

Kalkreuth W, Holz M, Mexias A, Balbinot M, Levandowski J, Willett J, Finkelman RB, Burger H (2010) Depositional setting, petrology and chemistry of Permian coals from the Paraná Basin: 2. South Santa Catarina Coalfield, Brazil. Int J Coal Geol 84:213–236

Karayigit AI, Gayer RA, Querol X, Onacak T (2000) Contents of major and trace elements in feed coals from Turkish coal-fired power plants. Int J Coal Geol 44:169–184

Kemezys M, Taylor GH (1964) Occurrence and distribution of minerals in some Australian coals. J Inst Fuel 37:389–397

Ketris MP, Yudovich YE (2009) Estimations of Clarkes for carbonaceous biolithes: world average for trace element contents in black shales and coals. Int J Coal Geol 78:135–148

Kislyakov YM, Shchetochkin VN (2000) Hydrogenic ore formation. Geoinformmark, Moscow, 608 p; (in Russian)

Lei J, Ren D, Tang Y, Chu X, Zhao R (1994) Sulfur-accumulating model of superhigh organosulfur coal from Guiding, China. Chin Sci Bull 39:1817–1821

Li YH (1982) A brief discussion on the mean oceanic residence time of elements. Geochim Cosmochim Acta 46:2671–2675

Li W, Tang Y (2013) Characteristics of the rare earth elements in a high organic sulfur coal from Chenxi, Hunan Province. J Fuel Chem Technol 41:540–549 (in Chinese with English abstract)

Li W, Tang Y (2014) Sulfur isotopic composition of superhigh-organic-sulfur coals from Chenxi Coalfield, southern China. Int J Coal Geol 127:3–13

Li D, Xu S (2000) Rotation-shearing genesis of metamorphic core complex—structure analysis of metamorphic core in Laojunshan, southeastern Yunnan Province. Geol Rev 46:113–119 (in Chinese with English abstract)

Li W, Tang Y, Deng X, Yu X, Jiang S (2013) Geochemistry of the trace elements in the high organic sulfur coals from Chenxi coalfield. J China Coal Soc 38:1227–1223 (in Chinese with English abstract)

Li J, Zhuang X, Querol X, Font O, Izquierdo M, Wang Z (2014a) New data on mineralogy and geochemistry of high-Ge coals in the Yimin coalfield, Inner Mongolia, China. Int J Coal Geol 125:10–21

Li X, Dai S, Zhang W, Li T, Zheng X, Chen W (2014b) Determination of As and Se in coal and coal combustion products using closed vessel microwave digestion and collision/reaction cell technology (CCT) of inductively coupled plasma mass spectrometry (ICP-MS). Int J Coal Geol 124:1–4

Liang H (2001) Experimental evidence for naturally occurring molecular chlorine (Cl_2) in organic phase of Chinese super-high sulfur coal. J Fuel Chem Technol 29:385–389 (in Chinese with English abstract)

Liu G, Yang P, Peng Z, Chou C-L (2004) Petrographic and geochemical contrasts and environmentally significant trace elements in marine-influenced coal seams, Yanzhou mining area, China. J Asian Earth Sci 23:491–506

Liu G, Zheng L, Wu E, Peng Z (2006) Depositional and chemical characterization of coal from Yayu Coal Field. Energy Explor Exploitation 24:417–437

Lowenstein TK, Hardie LA, Timofeev MN, Demicco RV (2003) Secular variation in seawater chemistry and the origin of calcium chloride basinal brines. Geology 31:857–860

Lyons PC, Palmer CA, Bostick NH, Fletcher JD, Dulong FT, Brown FW, Brown ZA, Krasnow MR, Romankiw LA (1989) Chemistry and origin of minor and trace elements in vitrinite concentrates from a rank series from the eastern United States, England, and Australia. Int J Coal Geol 13:481–527

Maksimova MF, Shmariovich EM (1993) Bedded-infiltrational ore formation. Nedra, Moscow (in Russian)

Marshall CE, Draycott A (1954) Petrographic, chemical and utilization studies of the Tangorin high sulphur seam, Greta Coal Measures, New South Wales. University of Sydney, Department of Geology and Geophysics Memoir 1954/1, 66 pp

McIntyre NS, Martin RR, Chauvin WJ, Winder CG, Brown JR, MacPhee JA (1985) Studies of elemental distributions within discrete coal macerals: use of secondary ion mass spectrometry and X-ray photoelectron spectroscopy. Fuel 64:1705–1711

Michard A, Albarède F (1986) The REE content of some hydrothermal fluids. Chem Geol 55:51–60

Oliveira MLS, Ward CR, Sampaio CH, Querol X, Cutruneo CMNL, Taffarel SR, Silva LFO (2013) Partitioning of mineralogical and inorganic geochemical components of coals from Santa Catarina, Brazil, by industrial beneficiation processes. Int J Coal Geol 116–117:75–92

Pearson DE, Kwong J (1979) Mineral matter as a measure of oxidation of a coking coal. Fuel 58:63–66

Peng S, Zhang J (1995) The coal-bearing depositional environment and its influence to mining of the Wuda Coalfield. Publishing House of China Coal. Industry, Beijing (in Chinese)

Price FT, Shieh YN (1979) The distribution and isotopic composition of sulfur in coals from the Illinois basin. Econ Geol 74:1445–1461

Qi H, Rouxel O, Hu R, Bi X, Wen H (2011) Germanium isotopic systematics in Ge-rich coal from the Lincang Ge deposit, Yunnan, Southwestern China. Chem Geol 286:252–265

Querol X, Fernández-Turiel JL, López-Soler A (1995) Trace elements in coal and their behaviour during combustion in a large power station. Fuel 74:331–343

Querol X, Alastuey A, Lopez-Soler A, Plana F, Zeng R, Zhao J, Zhuang X (1999) Geological controls on the quality of coals from the West Shandong Mining District, Eastern China. Int J Coal Geol 42:63–88

Rao CP, Gluskoter HJ (1973) Occurrence and distribution of minerals in Illinois coals. Ill State Geol Surv Circ 476:56

Raymond R Jr, Glandney ES, Bish DL, Cohen AD, Maestas L (1990) Variation of inorganic content of peat with depositional and ecological setting. In: Chyi LL, Chou C-L (eds) Recent advances in coal geochemistry: Geological Society of America, Special Paper 248

Reimann C, de Caritat P (1998) Chemical elements in the environment. Springer, New York, Inc., New York, 397 p

Ren DY (1996) Mineral matters in coal. In: Han DX (ed) Coal petrology of China. Publishing House of China Uni Min & Technol, Xuzhou, pp 67–77 (in Chinese with English abstract)

Ren D, Zhao F, Dai S, Zhang J, Luo K (2006) Geochemistry of trace elements in coal. Science Press, Beijing, 556pp; (in Chinese with English abstract)

Rietveld HM (1969) A profile refinement method for nuclear and magnetic structures. J Appl Crystallogr 2:65–71

Riley KW, French DH, Farrell OP, Wood RA, Huggins FE (2012) Modes of occurrence of trace and minor elements in some Australian coals. Int J Coal Geol 94:214–224

Rybin AV, Gur'yanov VB, Chibisova MV, Zharkov RV (2003) Rhenium exploration prospects on Sakhalin and the Kuril Islands Geodynamics, magmatism, and minerageny of the North Pacific Ocean. Magadan 3:180–183 (in Russian)

Seredin VV (2001) Major regularities of the REE distribution in coal. Dokl Earth Sci 377:250–253

Seredin VV, Dai S (2012) Coal deposits as a potential alternative source for lanthanides and yttrium. Int J Coal Geol 94:67–93

Seredin VV, Finkelman RB (2008) Metalliferous coals: a review of the main genetic and geochemical types. Int J Coal Geol 76:253–289

Seredin VV, Dai S, Sun Y, Chekryzhov IY (2013) Coal deposits as promising sources of rare metals for alternative power and energy-efficient technologies. Appl Geochem 31:1–11

Shand P, Johannesson KH, Chudaev O, Chudaeva V, Edmunds WM (2005) Rare earth element contents of high pCO_2 groundwaters of Primorye, Russia: mineral stability and complexation controls. In: Johannesson KH (ed) Rare earth elements in groundwater flow system. Springer, The Netherlands, pp 161–186

Shao L, Zhang P, Ren D, Lei J (1998) Late Permian coal-bearing carbonate successions in southern China: coal accumulation on carbonate platforms. Int J Coal Geol 37:235–256

Shao L, Jones T, Gayer R, Dai S, Li S, Jiang Y, Zhang P (2003) Petrology and geochemistry of the high-sulphur coals from the Upper Permian carbonate coal measures in the Heshan Coalfield, southern China. Int J Coal Geol 55:1–26

Skipsey E (1975) Relations between chlorine in coal and the salinity of strata water. Fuel 54:121–125

Smith JW, Batts BD (1974) The distribution and isotopic composition of sulfur in coal. Geochim Cosmochim Acta 38:121–133

Song D, Qin Y, Zhang J, Wang W, Zheng C (2007) Concentration and distribution of trace elements in some coals from Northern China. Int J Coal Geol 69:179–191

Spears DA (2005) A review of chlorine and bromine in some United Kingdom coals. Int J Coal Geol 64:257–265

Strauss H (2004) 4 Ga of seawater evolution: evidence from the sulfur isotopic composition of sulfate. In: Amend JP, Edwards KJ, Lyons TW (eds.), Sulfur biogeochemistry—past and present. Geological Society of America Special Paper, vol. 379, pp 195–205

Swaine DJ (1990) Trace elements in coal. Butterworths, London, 278 pp

Swanson SM, Engle MA, Ruppert LF, Affolter RH, Jones KB (2013) Partitioning of selected trace elements in coal combustion products from two coal-burning power plants in the United States. Int J Coal Geol 113:116–126

Tang X, Huang W (2004) Trace elements in Chinese coals. The Commercial Press, Beijing, pp 33–43 (in Chinese)

Taylor JC (1991) Computer programs for standardless quantitative analysis of minerals using the full powder diffraction profile. Powder Diffr 6:2–9

Taylor SR, McLennan SM (1985) The Continental Crust: its composition and evolution. Blackwell, London, 312 pp

Turner BR, Richardson D (2004) Geological controls on the sulphur content of coal seams in the Northumberland Coalfield, Northeast England. Int J Coal Geol 60:169–196

Van Der Flier E, Fyfe WS (1985) Uranium-thorium systematics of two Canadian coals. Int J Coal Geol 4:335–353

Vassilev SV, Eskenazy GM, Vassileva CG (2000) Contents, modes of occurrence and origin of chlorine and bromine in coal. Fuel 79:903–921

Wang W, Qin Y, Sang S, Jiang B, Zhu Y, Guo Y (2007) Sulfur variability and element geochemistry of the No. 11 coal seam from the Antaibao mining district, China. Fuel 86:777–784

Wang X, Dai S, Sun Y, Li D, Zhang W, Zhang Y, Luo Y (2011) Modes of occurrence of fluorine in the Late Paleozoic No. 6 coal from the Haerwusu Surface Mine, Inner Mongolia, China. Fuel 90:248–254

Wang X, Zhang M, Zhang W, Wang J, Zhou Y, Song X, Li T, Li X, Liu H, Zhao L (2012) Occurrence and origins of minerals in mixed-layer illite/smectite-rich coals of the Late Permian age from the Changxing Mine, eastern Yunnan, China. Int J Coal Geol 102:26–34

Ward CR (1980) Mode of occurrence of trace elements in some Australian coals. Coal Geol 2:77–98

Ward CR (2002) Analysis and significance of mineral matter in coal seams. Int J Coal Geol 50:135–168

Ward CR, Spears DA, Booth CA, Staton I, Gurba LW (1999) Mineral matter and trace elements in coals of the Gunnedah Basin, New South Wales, Australia. Int J Coal Geol 40:281–308

Ward CR, Matulis CE, Taylor JC, Dale LS (2001) Quantification of mineral matter in the Argonne Premium coals using interactive Rietveld-based X-ray diffraction. Int J Coal Geol 46:67–82

Ward CR, Li Z, Gurba LW (2007) Variations in elemental composition of macerals with vitrinite reflectance and organic sulphur in the Greta Coal Measures, New South Wales, Australia. Int J Coal Geol 69:205–219

Whateley MKG, Tuncali E (1995a) Quality variations in high-sulphur lignite of the Neogene Beypazari Basin, central Anatolia, Turkey. Int J Coal Geol 27:131–151

Whateley MKG, Tuncali E (1995b) Origin and distribution of sulphur in the Neogene Beypazari lignite basin, central Anatolia, Turkey. In: Whateley MKG, Spears DA (eds) European Coal Geology: Geological Society Special Publication, No. 82, pp 307–323

Wignall PB (1994) Black shales. Clarendon Press, Oxford, pp 1–127

Yossifova MG (2014) Petrography, mineralogy and geochemistry of Balkan coals and their waste products. Int J Coal Geol 122:1–20

Yudovich YE, Ketris MP (2005) Selenium in coal: a review. Int J Coal Geol 67:112–126

Zeng R, Zhuang X, Koukouzas N, Xu W (2005) Characterization of trace elements in sulphur-rich Late Permian coals in the Heshan coal field, Guangxi, South China. Int J Coal Geol 61:87–95